

No vertical axis rotations during Neogene transpressional orogeny in the NE Gobi Altai: coinciding Mongolian and Eurasian early Cretaceous apparent polar wander paths

Douwe J.J. van Hinsbergen,¹ Gijs B. Straathof,^{1,2} Klaudia F. Kuiper,^{2,3}
W. Dickson Cunningham¹ and Jan Wijbrans³

¹Department of Geology, University of Leicester, University Road, LE1 7RH Leicester, UK E-mail: hins@geo.uu.nl

²Paleomagnetic Laboratory 'Fort Hoofddijk', University of Utrecht, Budapestlaan 17, 3584 CD Utrecht, the Netherlands

³Department of Isotope Geochemistry, VU Amsterdam, De Boelelaan 1085, 1081 HV Amsterdam, the Netherlands

Accepted 2007 December 18. Received 2007 September 7; in original form 2007 April 4

SUMMARY

In this paper, we test the role of vertical axis rotations during transpressional mountain building. To this end, we carried out a palaeomagnetic study in the NE Gobi Altai of southern Mongolia, sampling widely exposed lower Cretaceous lavas allowing comparison of rotation histories of the Ih Bogd, Baga Bogd and Artz Bogd restraining bends at the eastern termination of the Bogd strike-slip zone. We provide new ⁴⁰Ar/³⁹Ar ages to show that the stratigraphy of mafic lavas and fluvio-lacustrine sediments on the southern flanks of Mt Ih Bogd and Mt Baga Bogd have ages between ~125 and ~122 Ma, and a mafic sill that intrudes the sequence has an age of 118.2 ± 0.8 Ma. The lavas are older than previously dated lavas south of Artz Bogd, with ages of 119–115 Ma. Palaeomagnetic results from the 119–115 Ma lavas south of Artz Bogd show a significant steeper inclination than both results from 125 to 122 Ma lavas of Baga Bogd and Ih Bogd, as well as from newly sampled and previously published younger lavas and necks of the 107–92 Ma Tsost Magmatic Field and Shovon and Khurmen Uul basalts. We explain this result by insufficient averaging of secular variation and small errors induced by overcorrection of bedding tilt. We show that individual lavas in the SE Artz Bogd locality represent individual spot readings of the Earth's magnetic field and integrate all results obtained from lower Cretaceous lavas in the Gobi Altai. We present a pole, or rather, an apparent polar wander path without significant plate motion from the reference positions of Eurasia, from ~125 to 95 Ma, with $n = 126$, $\lambda = 80.8^\circ$, $\phi = 158.4^\circ$, $\kappa = 25.3$, $A95 = 2.5$, palaeolatitude = 48.2 with a scatter $S\lambda = 16.7$ ($S\lambda = 15.3$, $S\phi = 17.8$) and a regionally consistent direction for the Gobi Altai of $D/I = 11.1^\circ/65.9^\circ$, $\Delta D/\Delta I = 3.8^\circ/1.9^\circ$. This is one of the best-determined palaeopoles/APWP's for Asia. Formation of the Ih Bogd, Baga Bogd and Artz Bogd restraining bends was thus not associated with vertical axis rotations larger than our error margin of ~10°. From this we conclude that the Bogd strike-slip zone is a weak fault zone, in which shear is localized.

Key words: Palaeomagnetism applied to tectonics; Continental tectonics: strike-slip and transform; Asia.

1 INTRODUCTION

Transpressional mountain belts form a distinct and unique class of orogen, in which high elevations can be established with relatively small amounts of thrust displacement compared to collisional and subduction related orogens in active margin settings (Scotese 2001; Cunningham 2005; van Hinsbergen *et al.* 2005; Hafkenscheid *et al.* 2006). This is because transpressional ranges typically are sites of combined thrusting, strike-slip and oblique-slip displacements and high-angle faults with dip-slip components are, therefore, common (Cunningham 2005). High mountain ranges associated with regional

strike-slip fault systems where transpressional deformation plays a significant role commonly have full or half-flower structure fault geometries and occur in continental transform settings (e.g. Southern Alps, New Zealand; Transverse Ranges, California and Lebanon Ranges) and along intracontinental, intraplate strike-slip systems (e.g. the Denali Range, Alaska; Altyn Tagh fault system in Tibet, and the Altai and Gobi Altai ranges, see also the review of Kim & Sanderson 2006).

The Altai and Gobi Altai mountains in Mongolia form one of the world's largest linked intracontinental transpressional orogens (Cunningham 2005). The India–Asia collision led to intraplate

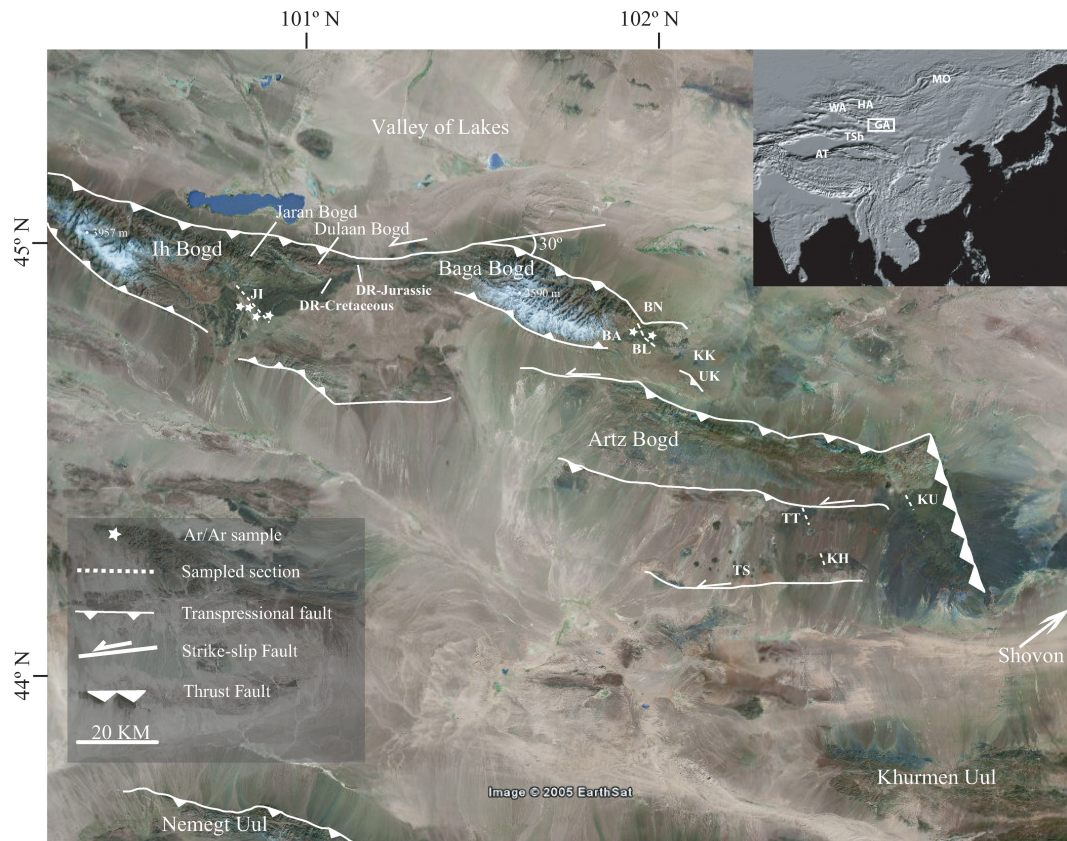


Figure 1. Earth Sat image of the Gobi Altai with the main structural elements and sampling locations. Locality Shovon of Hankard *et al.* (2007b) is located to the east of Artz Bogd. Inset: AT = Altyn Tagh fault; BA = Baga Bogd sites; BL = Bulgantiin Uul sites (see Fig. 2); BN = Bulgantiin Uul North sites; DR = Dulaan Bogd sites; GA = Gobi Altai; HA = Hangay Dome; JI = Jaran Bogd sites (see Fig. 2); KH = Khatavch sites; KK = Khalzan Khairkhan sites (see Fig. 2); KU = Kharaat Uul sites; MO = Mongol-Okhotsk suture zone; TS = Tsost Magmatic Field sites; Tsh = Tien Shan, TT = Tsagaan Tsav sites; UK = Unegt Khairkhan sites; WA = Western Altai.

deformation in central Asia, which extended progressively northward through Tibet and the Tien Shan into Mongolia (Tapponnier & Molnar 1979; Cobbold & Davy 1988). In western and Central Mongolia, two transpressional orogenic belts formed around a passive indenter formed by the Hangay dome (Cunningham 1998, 2005; Fig. 1): the right-lateral Mongolian Altai in the west (Cunningham *et al.* 1996b, 2003a), which formed since the Oligocene (Howard *et al.* 2003, 2006) and the left-lateral Gobi Altai in the south (Cunningham *et al.* 1996a, 1997), which formed since the late Miocene (~8 Ma; Vassallo *et al.* 2007). In both ranges, deformation continues today (Baljinnyam *et al.* 1993; Ritz *et al.* 1995; Bayarsayhan *et al.* 1996; Carretier *et al.* 1998, 2002; Philip & Ritz 1999; Ritz *et al.* 2003; Vassallo *et al.* 2005). Both belts contain linked strike-slip faults, thrust ridges and restraining bends, the latter leading to lenticular, well-exposed mountain ranges with elevations up to 4 km, as much as 2.5 km higher than the surrounding basins.

The origin of intracontinental transpressional mountain ranges is debated: if there is a compressional component across the master strike-slip fault system, it may lead to localized thrusting and vertical axis rotation of the fault, such as proposed in the concept of discrete block rotations within a distributed fault system (Garfunkel 1988; Nur *et al.* 1988; Taylor *et al.* 1998; Bayasgalan *et al.* 1999; Cunningham 2005). Bayasgalan *et al.* (1999) proposed that restraining bend formation at the northeastern termination of the Gobi Altai resulted from clockwise rotation of 'slats' bound by parallel left-lateral strike slip faults, comparable to scenarios in-

voked for Aegean region fault rotations (Taymaz *et al.* 1991). At present, the angle between the transpressional segments bounding the restraining bends and purely strike-slip fault segments in between restraining bends in the NE Gobi Altai is approximately 20–30° (Fig. 1). Alternatively, strike-slip segments may initially form in an echelon pattern and across contractional segments. Both the strike-slip segments and the contractional segments may form due to reactivation of favourably oriented basement faults and structural 'grain'. In this paper, we test by means of palaeomagnetic analysis whether transpressional mountain building in the NE Gobi Altai mountain range of southern Mongolia was associated with vertical axis rotations.

To this end, we targeted the youngest stratigraphic interval with widespread exposure across the NE Gobi Altai region, with suitable lithologies for palaeomagnetic analysis that predates the late Miocene (~8 Ma; Vassallo *et al.* 2007) onset of uplift of the restraining bends of Ih Bogd, Baga Bogd and Artz Bogd (Vassallo *et al.* 2007; Fig. 1). The Phanerozoic geological history of southern Mongolia preceding the formation of the modern transpressional mountain ranges consists of multiple tectonic events broadly reducible to three major phases: (1) Mainly Palaeozoic accretion of terranes of continental and oceanic affinity (Sengör *et al.* 1993; Buchan *et al.* 2001, 2002; Badarch *et al.* 2002; Dijkstra *et al.* 2006; Helo *et al.* 2006; Windley *et al.* 2007) ending in the late Jurassic with the closure of the last intra-Asian 'Mongol-Okhotsk' ocean between Mongolia and Siberia, the last intra-Asian seaway within the Altai

(Zhao *et al.* 1990; Enkin *et al.* 1992; van der Voo *et al.* 1999; Zorin 1999; Cogné *et al.* 2005; Windley *et al.* 2007). Terrane accretion caused a roughly E–W trending basement grain in the Gobi Altai region; (2) Mesozoic rifting and widespread basin formation, clastic sedimentation and volcanism, notably in the late Jurassic and early Cretaceous (Berkey & Morris 1927; Graham *et al.* 1993; Traynor & Sladen 1995; Hendrix *et al.* 1996; Meng *et al.* 2003; Johnson 2004; Wang *et al.* 2006) and (3) scattered occurrences of Cenozoic basaltic magmatism and local sedimentary basin formation (Whitford-Stark 1987; Devyatkin & Smelov 1980; Höck *et al.* 1997; Barry & Kent 1998; Cunningham 2001; Barry *et al.* 2003). In the NE Gobi Altai region, all elements of this general history are found in the rock record. The restraining bends of Ih Bogd, Baga Bogd and Artz Bogd expose the pre-Mesozoic basement in their cores and are flanked by lower Cretaceous alternating lavas and fluvio-lacustrine sediments, which reach an exposed thickness up to 1500 m or more, notably along their southeastern sides (Fig. 1). Furthermore, scattered occurrences of shallow intrusive basalts, basalt plateaux and younger lavas have been reported (Devyatkin & Smelov 1980; Barry & Kent 1998; Barry *et al.* 2003; Hankard *et al.* 2007a). However, the occurrences of the Cenozoic volcanic rocks are too few and scattered for regional correlation and assessment of vertical axis rotations. Therefore, we targeted the lower Cretaceous stratigraphy, which consists dominantly of basalts for our palaeomagnetic and geochronologic investigations.

Recently, Cogné *et al.* (2005) concluded that the closure of the Mongol-Okhotsk ocean occurred in the late Jurassic, a finding that was confirmed by Hankard *et al.* (2007b). Therefore, we tested for regional vertical axis rotations by comparing our palaeomagnetic results with apparent pole positions of stable Eurasia in the early Cretaceous published by Besse & Courtillot (2002), Schettino & Scotese (2005) and Torsvik *et al.* (in press).

2 GEOLOGY AND SAMPLING

We collected 871 samples from 123 lava and magmatic neck sites, with typically seven samples per site (Fig. 1). The southeastern parts of these three mountain ranges expose the Mesozoic stratigraphy that was the target of this study.

The Mesozoic deposits comprise some lavas sampled near Dulaan Bogd (DR-Jurassic) predating the early Cretaceous, and which are estimated as Jurassic. Along their southern edges, the basement exposed in the Ih Bogd, Baga Bogd and Artz Bogd restraining bends is overlain by lavas and fluvio-lacustrine deposits of early Cretaceous age. Palaeoflow directions in fluvial sediments, as well as the lateral disappearance of lavas to the east and west suggest a half-graben geometry with north-facing normal faults and southward palaeoslopes. This has an important implication: lavas may have had an initial non-tectonic tilt of a few degrees to the south. However, tilting of lacustrine mudrocks in between lavas, as well as observed tilted Tertiary peneplains suggest that at least part of the generally 10–15° of southward tilt, which characterizes the lava successions is of tectonic, post-depositional origin. We thus chose to correct the palaeomagnetic directions obtained in this study for bedding tilt and test the validity of this with fold tests, although we note that this may lead to a structural overcorrection of a few degrees to the north if the successions were not deposited purely horizontally.

The southeastern part of Ih Bogd exposes a southeastward tilted and locally tectonically folded sequence of lower Cretaceous lavas and sediments, continuously exposed over 20 km, from Dulaan Bogd (DR-Cretaceous) to Jaran Bogd (JI), sometimes also transcribed

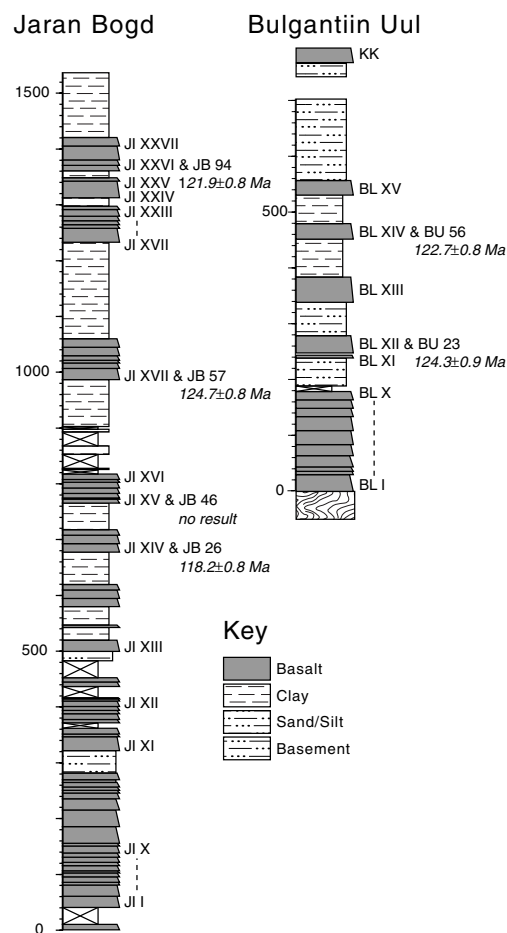


Figure 2. Logs of the Jaran Bogd and Bulgantiin Uul sections with palaeomagnetic and stratigraphic sampling levels.

as Jiran or Dziran Bogd (Fig. 1). Chilled margins at the base of the lavas, pahoehoe flow structures, local pillow structures, and upward increasing vesicularity leading to distinct erosion profiles show that the basalts in this section are largely extrusive, although a few bedding-parallel sills are also suspected. From the Jaran Bogd section, we collected three samples JB26, JB57 and JB94 for $^{40}\text{Ar}/^{39}\text{Ar}$ dating (Fig. 2). Alluvial and fluvial sediments and lavas of late and post-Cretaceous age unconformably overlie the sequence.

The region east of Baga Bogd contains a stratigraphic succession of Cretaceous lavas and sediments, which were sampled at four locations (BA, BL, BN, KK). We collected two samples from the Bulgantiin Uul (BL) section—samples BU23 and BU56—for $^{40}\text{Ar}/^{39}\text{Ar}$ geochronology (Fig. 2). In between the eastern end of Baga Bogd and Artz Bogd to the south, we collected samples from seven steeply dipping lavas in the footwall of a NE-verging thrust at Unegt Khairkhan (UK; Fig. 1).

South of Artz Bogd, lower Cretaceous lavas, alternating with light blue and white lacustrine clays and redbeds are exposed. These sequences are intruded by the Tsost Magmatic Field basaltic necks (Whitford-Stark 1987; Devyatkin & Smelov 1980; Barry 1999; Hankard *et al.* 2007b). Barry (1999) reported $^{40}\text{Ar}/^{39}\text{Ar}$ ages of the lavas ranging from 119 to 115 Ma, and ages from the intrusions in the Tsost Magmatic Field ranging from 107 to 96 Ma. We sampled the lavas in the continuous 119–117 Ma Tsagaan Tsav section (TT) of Barry (1999) and in its lateral equivalent Kharaat Uul (KU), as well as near the top of the stratigraphy, at Khatavch

(115 Ma; Barry 1999). West of these sections, we sampled 10 sites in the Tsost Magmatic Field. Recently, Hankard *et al.* (2007b) also reported palaeomagnetic results from the Tsost Magmatic Field. They described their sampling locations as both necks and flows and reported K/Ar ages of ~104–94 Ma, with one outlier at 118 Ma. These ages suggest that the majority of their sites were taken from the basalt intrusions of 107–96 Ma (Barry 1999) or 104–94 Ma (Hankard *et al.* 2007b), with the 118 Ma age probably obtained from the underlying lavas equivalent to the series east of the Tsost Magmatic Field with ages of 119–115 Ma (Barry 1999; Fig. 1).

3 GEOCHRONOLOGY

Six basalts were sampled for $^{40}\text{Ar}/^{39}\text{Ar}$ dating (Fig. 1). Microscopic inspection showed no or hardly any signs of alteration. Groundmass was separated using standard mineral separation techniques. All samples were leached with 1 N HNO_3 during 1 hour in an ultrasonic bath. Circa 50 mg of material from the size fraction 250–500 μm of the groundmass of each sample was wrapped in Al-foil and loaded in a 15 mm ID quartz vial. The in-house Drachenfels sanidine standard (25.26 ± 0.03 Ma; modified from Wijbrans *et al.* (1995) was used as neutron fluence monitor and loaded at top and bottom positions between each set of four unknowns. Samples and standards were irradiated for 18 hr in the Cd-lined RODEO P3 position of the HFR Petten, the Netherlands. $^{40}\text{Ar}/^{39}\text{Ar}$ incremental heating experiments were performed at the Vrije Universiteit Amsterdam. Standards were fused with a Synrad 48–5 50W CO_2 laser. Samples load in a sample tray with 6 mm diameter holes in which the sample was spread out evenly and were incrementally heated using a Raylase scan head as a beam delivery and beam diffuser system. After purification the gas was analysed with a Mass Analyzer Products LTD 215–50 noble gas mass spectrometer. Beam intensities were measured in a peak-jumping mode in 0.5 mass intervals over the mass range 40–35.5 on a Balzers 217 secondary electron multiplier. System blanks were measured every four steps. Mass discrimination was monitored by frequent analysis of aliquots of air. The irradiation parameter J for each unknown was determined by interpolation using a second-order polynomial fitting between the individually measured standards. Ages are calculated using the in-house developed ArArCalc software (Koppers 2002). All $^{40}\text{Ar}/^{39}\text{Ar}$ ages are calculated with Steiger & Jäger (1977) decay constants at the 2 level and include the analytical error and error in J . Corrections factors for neutron interference reactions are $2.7 \pm 0.03 \times 10^{-4}$ for $(^{36}\text{Ar}/^{37}\text{Ar})_{\text{Ca}}$, $6.99 \pm 0.13 \times 10^{-4}$ for $(^{39}\text{Ar}/^{37}\text{Ar})_{\text{Ca}}$ and $1.83 \pm 0.2 \times 10^{-2}$ for $(^{40}\text{Ar}/^{39}\text{Ar})_{\text{K}}$.

Table 1 summarizes the $^{40}\text{Ar}/^{39}\text{Ar}$ results. The full analytical data are given in the supplementary Table S1. The general criterion for definition of a reliable plateau age is that the plateau includes more than three concordant incremental heating steps representing more than 50 per cent of total $^{39}\text{Ar}_{\text{K}}$ released (e.g. Fleck *et al.* 1977). The MSWD over the plateau steps was calculated as an additional test for plateau homogeneity. Acceptable plateaus yield MSWD values of less than 2.0. Five samples yield excellent age plateaus according to these criteria and do not show indications of thermal disturbances. One sample yields no reliable age spectra. Its total fusion age of 166 Ma (JB46) does not have any geologically meaningful and this age is not included in further analysis. The $^{40}\text{Ar}/^{36}\text{Ar}$ intercepts of the inverse isochrons do not deviate from the atmospheric $^{40}\text{Ar}/^{36}\text{Ar}$ ratio of 295.5 at the 2σ level and show no indications of inherited argon components (Table 1 and Fig. 3). The radiogenic ^{40}Ar contents are generally high with all plateau steps >80 per cent $^{40}\text{Ar}^*$,

Table 1. Summary of $^{40}\text{Ar}/^{39}\text{Ar}$ results.

Irradiation ID	Sample	Lab ID	J (± 0.3 per cent)	Plateau age (Ma)	MSWD	N	$^{39}\text{Ar}_{\text{K}}$ (per cent) in plateau	$^{40}\text{Ar}^*$ (per cent)	K/Ca	Total fusion age (Ma)	Inverse isochron intercept
VU62-A3	BU23	07m×077	0.005325	124.3 \pm 0.9	1.52	8 (5)	81.0	88.5	0.41 \pm 0.05	124.6 \pm 0.9	311 \pm 25
VU62-A4	BU56	07m×078	0.005324	122.7 \pm 0.8	1.40	8 (5)	75.2	92.8	0.50 \pm 0.07	123.5 \pm 0.8	291 \pm 30
VU62-A5	JB26	07m×079	0.005321	118.2 \pm 0.8	1.38	8 (5)	72.5	95.1	0.15 \pm 0.04	120.7 \pm 1.0	275 \pm 66
VU62-A6	JB46	07m×081	0.005318	No plateau	–	13	–	96.8	0.26 \pm 0.04	165.9 \pm 1.0	9565 \pm 57 955 ^a
VU62-A8	JB57	07m×082	0.005313	124.7 \pm 0.8	1.82	9 (4)	82.9	89.2	0.26 \pm 0.05	127.0 \pm 0.8	310 \pm 14
VU62-A9	JB94	07m×083	0.005310	121.9 \pm 0.8	1.68	6 (7)	63.8	93.0	0.30 \pm 0.08	112.7 \pm 0.8	318 \pm 32

Notes: MSWD is mean square weighted deviates, N is the number of steps included (excluded) in the plateau age. $^{39}\text{Ar}_{\text{K}}$ (per cent) is the percentage of $^{39}\text{Ar}_{\text{K}}$ released by plateau steps. $^{40}\text{Ar}^*$ is the radiogenic amount of ^{40}Ar . Total fusion ages and inverse isochron intercepts are given for reference. Errors are given at 95 per cent confidence level.

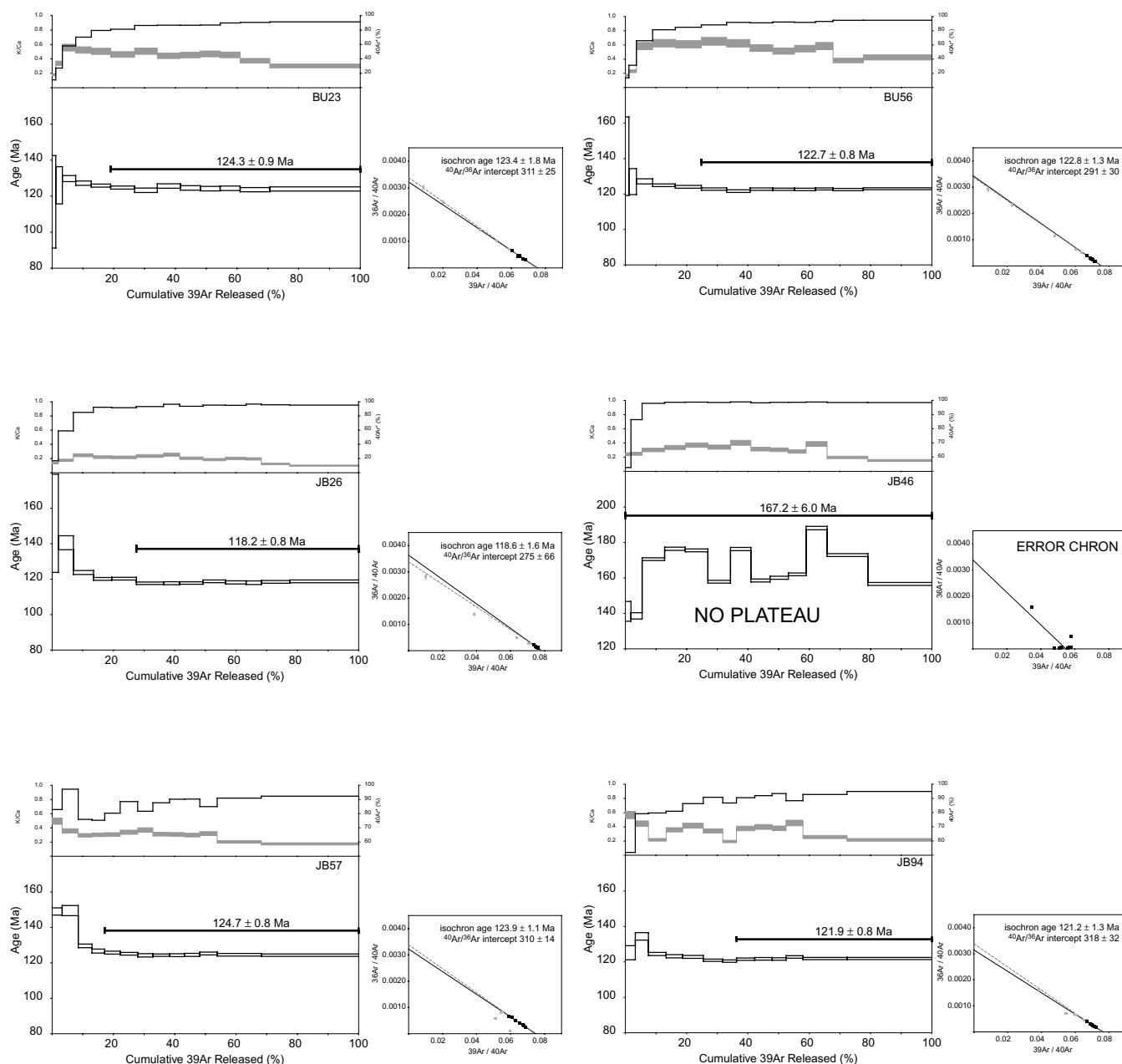


Figure 3. Incremental heating $^{40}\text{Ar}/^{39}\text{Ar}$ spectra of eight basalt samples. The width of the bars/steps represents the 2σ analytical error. On top the K/Ca ratio (grey area, width is 2σ error) and amount of radiogenic $^{40}\text{Ar}^*$ (black line) are displayed. Weighted mean plateau ages are given. The small insets show the inverse isochron diagrams. ^a = error chron.

but most even >90 per cent $^{40}\text{Ar}^*$. Therefore, we conclude that alteration, if present has been successfully removed by leaching and interpret the weighted plateau ages as the best age estimates for the 5 basalts (Table 1, Fig. 3).

4 PALAEOMAGNETIC PROCEDURES

Samples were collected with a water-cooled gasoline powered motor drill and cut in pieces of an inch across and length in the laboratory. The orientation of all samples was measured with both a magnetic and a sun compasses. To exclude any local magnetic deviations, all palaeomagnetic interpretations are based on the solar azimuths. The

samples were demagnetized using either thermal (TH) or alternating field (AF) progressive demagnetization. Heating took place in a magnetically shielded, laboratory-built furnace using small temperature increments of $20\text{--}80^\circ\text{C}$ up to temperatures of 640°C . The AF demagnetization was carried out with $5\text{--}20$ mT increments up to 120 mT. For all samples, the natural remanent magnetization (NRM) of the specimens was measured on a 2G Enterprises horizontal DC SQUID cryogenic magnetometer (noise level 3×10^{-12} Am²). For AF demagnetization, the instrument was interfaced with an in-home developed robot-assisted automated measuring device.

To identify the magnetic carriers and their characteristics, acquisition of isothermal remanent magnetization (IRM) was carried out (Fig. 4). Samples were carefully selected based on the

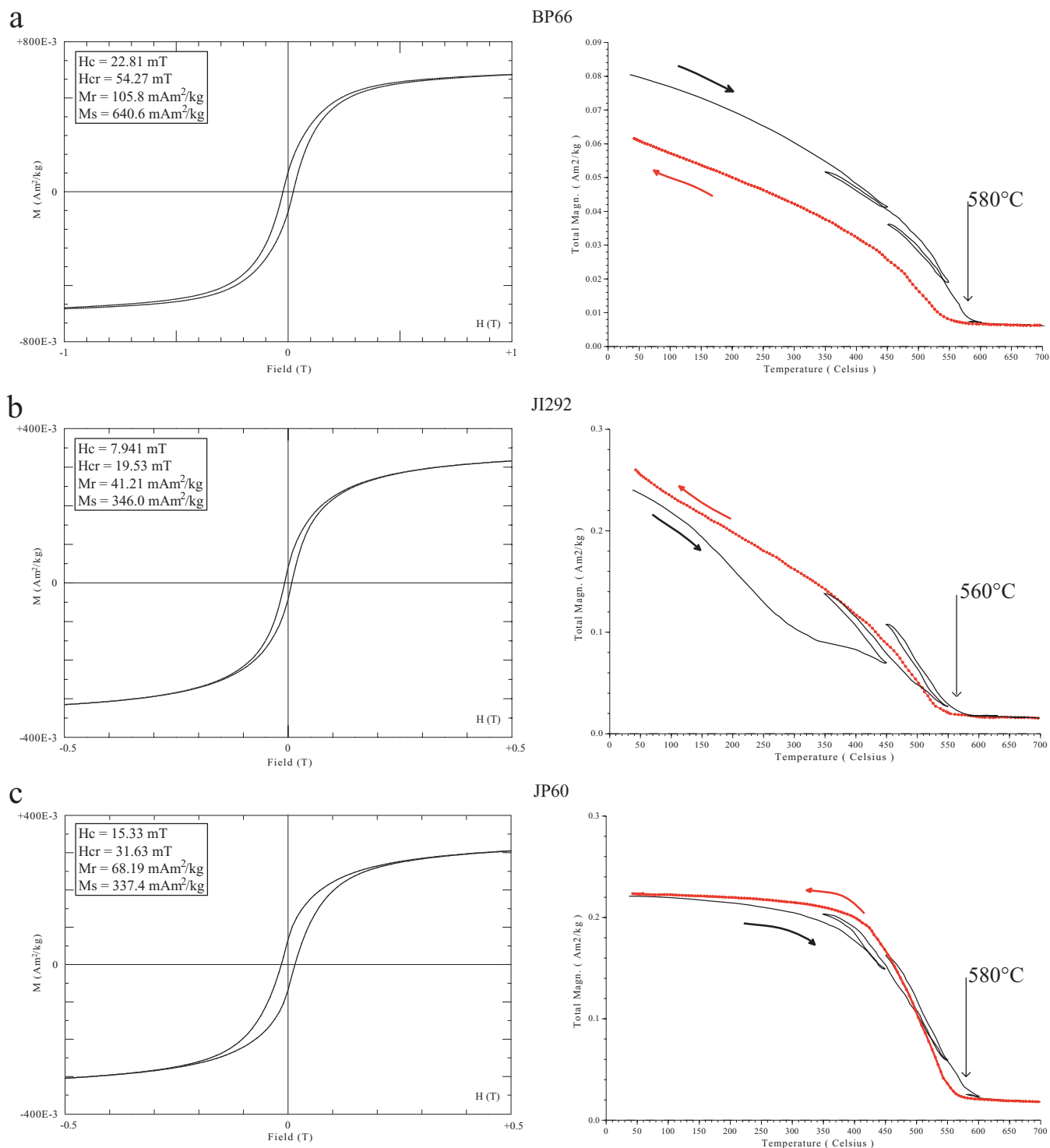


Figure 4. Rock magnetic properties are presented by hysteresis loops and thermomagnetic curves of three different samples. The thin shape of the hysteresis loops indicates the presence of (pseudo-)single domain grains. The loops closing at 0.3 Tesla in (b) and (c) indicate (titano-)magnetite as the dominant carrier. The thermomagnetic curves of the three samples reveal blocking temperatures of 560–580 °C, again indicative of (titano-)magnetite as main magnetic carrier.

demagnetization diagrams. They served as being representative for lightning struck samples (JP60), samples that were entirely demagnetized at ± 580 °C (BP66) and at ± 560 °C (JI292). Additionally, hysteresis loops were determined (Fig. 4). The plots of M_r/M_s against H_{hc}/H_c in a Day-plot (Day *et al.* 1977), indicates the presence of pseudo-single-domain grains in all three analysed samples;

(Fig. 5). Curie temperatures were determined using a modified horizontal translation type Curie balance that applies a cycling field (Mullender *et al.* 1993). Stepwise increasing temperatures of 450, 550, 600, 650 and 700 °C were used revealing blocking temperatures of 560–580 °C (Fig. 4). These Curie temperatures, together with the hysteresis loops closing at or below ~ 0.3 Tesla, indicate (Ti-poor)

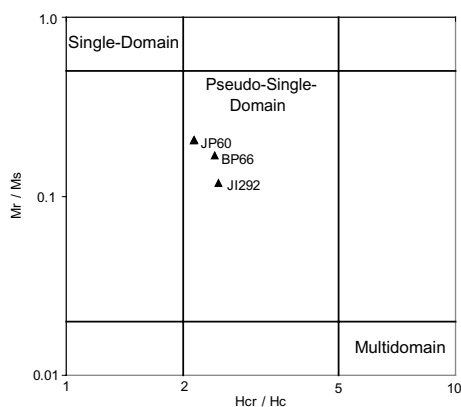


Figure 5. Day-plot of the hysteresis parameters of the studied samples (after Dunlop 2002).

magnetite to be the main carrier of the natural remanent magnetization (NRM). Finally, these rock magnetic experiments give us confidence that we measured a stable NRM.

The demagnetization diagrams of the NRM were plotted in orthogonal vector diagrams (Zijderveld 1967). In addition, a number of multicomponent samples were plotted on equal-area projections. Representative examples are given in Fig. 6. Identification of the characteristic remanent magnetization (ChRM) was done by principal component analysis (Kirschvink 1980). When vector end points showed a trend towards the origin of the diagram, we determined this component to be the ChRM.

Initially, we demagnetized one sample of every site by thermal demagnetization. The remaining samples of the sites were either demagnetized on a robotized alternating field demagnetizer or demagnetized thermally. Initial intensities range typically from 0.5 to 2.0 A m⁻¹. The AF demagnetized samples show good agreement with the TH samples of the same site (Figs 6c and d). At a number of sites, the ChRM was not recognized in the TH demagnetization but could clearly be determined by AF demagnetization (Figs 6k and l).

5 ANALYSIS

Samples were rejected from further analysis if the maximum angular deviation exceeded 15°. Because lava sites represent spot-readings of the Earth's magnetic fields, within-site errors can be assumed to be random, and averages and cones of confidence on lava site level were determined by Fisher statistics (Fisher 1953). The resulting site means and statistical values are given in Table 2. We excluded lava sites with $k < 50$ from further analysis, since variation between samples within a single lava should be minimal. Remaining lava sites were screened for remagnetization (e.g. caused by lightning). Complete remagnetization of sites was recognized in 15 cases. The declinations of the lowermost sites of section II show remarkable deviations from north after tectonic correction. These sites show consistent reversed directions before tectonic correction and we interpret this as a post-folding obtained NRM, which is confirmed by the clearly negative foldtest of Tauxe & Watson (1994; Fig. 7a). The results of this foldtest indicate that the best fit is found much below 0 per cent untilting. This may be the result of various degrees of overprinting or uncertainties in bedding attitudes. These sites were excluded from further analyses. Nine sites show complete remagnetization caused by lightning. The NRM of rocks struck by lightning can be entirely or partly overprinted (Hallimond & Herron 1933).

The identification of lightning-induced NRM is based on abnormal high magnetic intensity, together with within-site randomness of NRM directions (Fig. 6i). In some cases, an overprint caused by lightning or gyro-remanent remagnetization (Dankers & Zijderveld 1981) could be identified and eliminated. This was done using the great-circle approach of (McFadden & McElhinny 1988; Fig. 6).

Because scatter of palaeomagnetic directions induced by secular variation of the Earth's magnetic field is near-Fisherian at the poles, but ellipsoid elsewhere on the globe (Cox 1969; Tauxe & Kent 2004), we calculated our lava site means into poles and determined locality means on the poles using Fisher-statistics (Fisher 1953). Lava sites were excluded from determination of locality means when their poles exceeded the maximum angular standard deviation of Vandamme (1994; Table 2). The average pole was then calculated into an average declination and inclination, with an errorbar ΔD and ΔI following equations A.60 and A.57 of Butler (1992), respectively (Table 2). The resulting average directions per sampling locality are shown in Figs 8 and 9.

Although the lava site averages of locality Dulaan Bogd Jurassic are very accurate, site averages are scattered and do not pass the reversal test of McFadden & McElhinny (1990). The resulting k -value of 2.7 indicates that there is no sensible palaeomagnetic direction obtained from these 10 lavas and they are excluded from further analyses. The average direction obtained from the lower Cretaceous lavas at Unegt Khairkhan suggest very large rotations which can by no means be confirmed through structural geological observations, and we interpret these results (based on only three of the seven lavas) as bearing of no regional importance. These directions are excluded from further analyses.

In the following analysis, we integrate our results from lower Cretaceous with the recently published results of Hankard *et al.* (2005, 2007b), and recalculated the average pole since our cut-off of $k = 50$ for individual lava sites eliminates a few of their sites, and mainly because we use a fundamentally different statistical approach by calculating averages on poles and calculating ΔD and ΔI , instead of determining a dp/dm error ellipsoid around the (Fisherian) average pole. Based on age and location, we identify five localities: SE Ih Bogd ($n = 21$, 124.7–118.2 Ma), SE Baga Bogd ($n = 29$, 124.3–122.7), SE Artz Bogd ($n = 24$, 119.3–115.4 Ma; Barry 1999), the Tsost magmatic field, from which we obtained seven reliable site means, and which is combined with the recently published 'Artz Bogd' locality of Hankard *et al.* (2007b) ($n = 25$, 107–94.7 Ma) and finally the combined Shovon/Khurmen Uul locality of Hankard *et al.* (2005, 2007b); $n = 20$, 94.7–92 Ma). Within all three localities SE Ih Bogd, SE Baga Bogd and SE Artz Bogd we have sampled limbs of steep folds and the resulting positive fold tests (Fig. 7) show that folding and tilting (largely) post-dates deposition and acquisition of the NRM.

Testing of common true mean directions (McFadden & Lowes 1981) shows that there is neither significant difference at the 95 per cent confidence level between the SE Ih Bogd and SE Baga Bogd localities, nor between the Tsost Magmatic Field and the Shovon/Khurmen Uul localities (Table 3). Therefore, we have recalculated the palaeopoles and average directions and combined the above localities (Table 4). However, locality SE Artz Bogd does differ from the older and younger combined localities of Ih Bogd/Baga Bogd and Tsost/Shovon/Khurmen Uul (Table 3). The combined localities of Ih Bogd/Baga Bogd and Tsost/Shovon/Khurmen Uul, however, do not significantly differ at the 95 per cent confidence level. In Table 4, we have combine all our successful data to end up with a combined early Cretaceous pole of the Gobi Altai ($n = 126$, ~125–94 Ma).

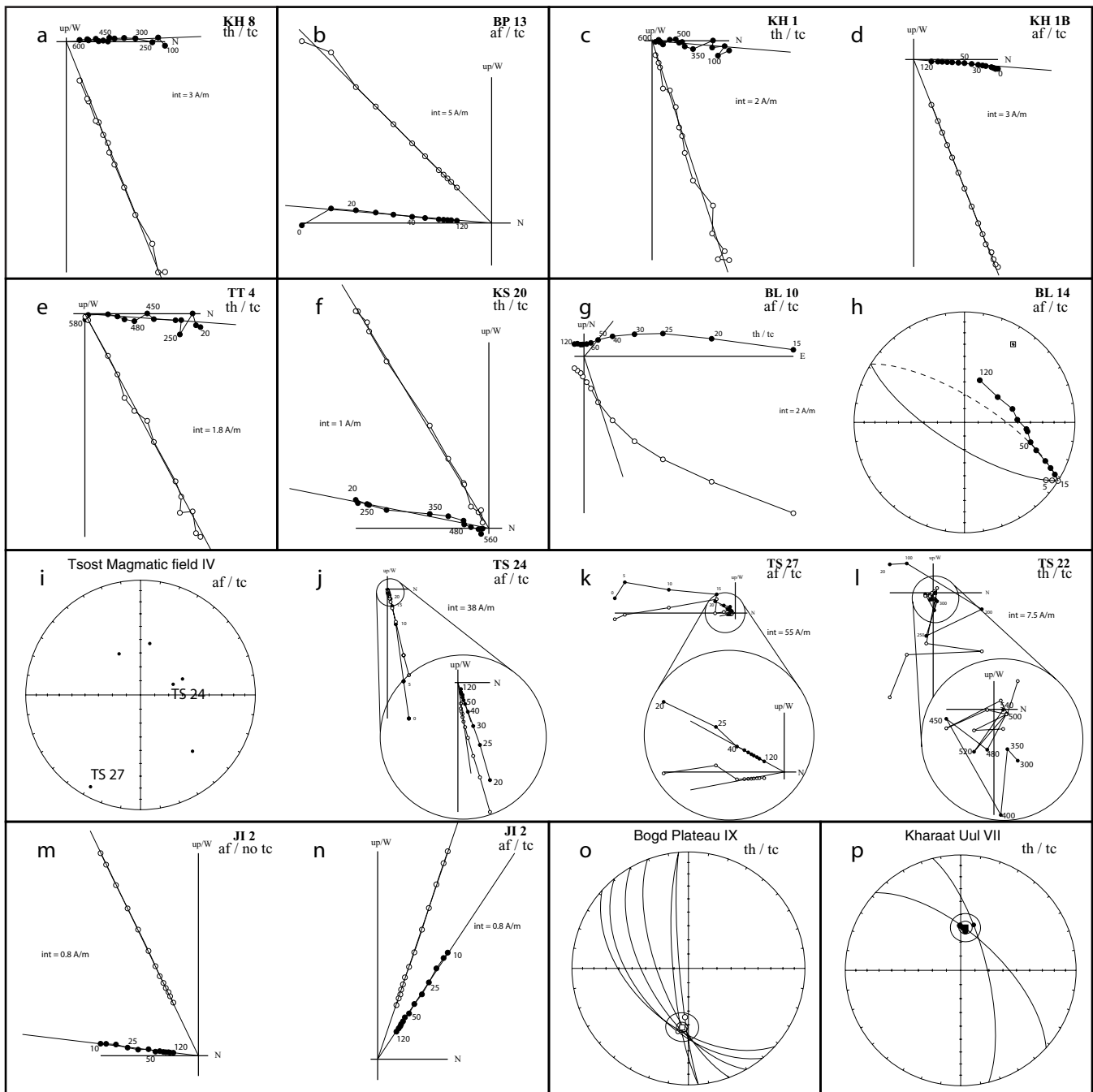


Figure 6. Representative aspects of demagnetization. (a) Zijderveld diagram showing typical thermal (TH) demagnetization results; (b) Zijderveld diagram showing typical alternating field (AF) demagnetization results; (c and d) TH and AF demagnetization yield comparable results; (e and f) typical normal (e) and reversed (f) palaeomagnetic directions. Reversed directions are found in only two lavas in the Bulgantiin Uul section. (g) Gyro-remanent magnetization (Dankers & Zijderveld 1981); (h) eliminating the effects of gyro-remanent magnetization by applying the great-circle method of McFadden & McElhinny (1988); (i) equal area projection of palaeomagnetic directions in a lightning-struck lava site; (j, k and l) examples of Zijderveld diagrams of lightning-struck site TS IV of Fig. 6i; (m and n) Total remagnetization of a sample, showing a ‘normal’ reversed direction prior to tilting (m) and an anomalous declination after tilt correction (n); (o and p) examples of lightning-struck sites where the use of great circles allowed the reconstruction of the ChRM.

To determine whether post-Cretaceous rotations have occurred in the Gobi Altai, we compare our directions with palaeomagnetic poles constructed for stable Eurasia. In recent years, three apparent polar wander paths (APWP’s) have been reconstructed for Eurasia by Besse & Courtillot (2002), Schettino & Scotese (2005) and

Torsvik *et al.* (in press). We compare our results to the published poles and directions predicted for the Gobi Altai from these three reference models at 90, 100, 110, 120 and 130 Ma (Table 5). All localities in the Gobi Altai except for SE Artz Bogd share a common true mean direction with their relevant reference poles (Table 6).

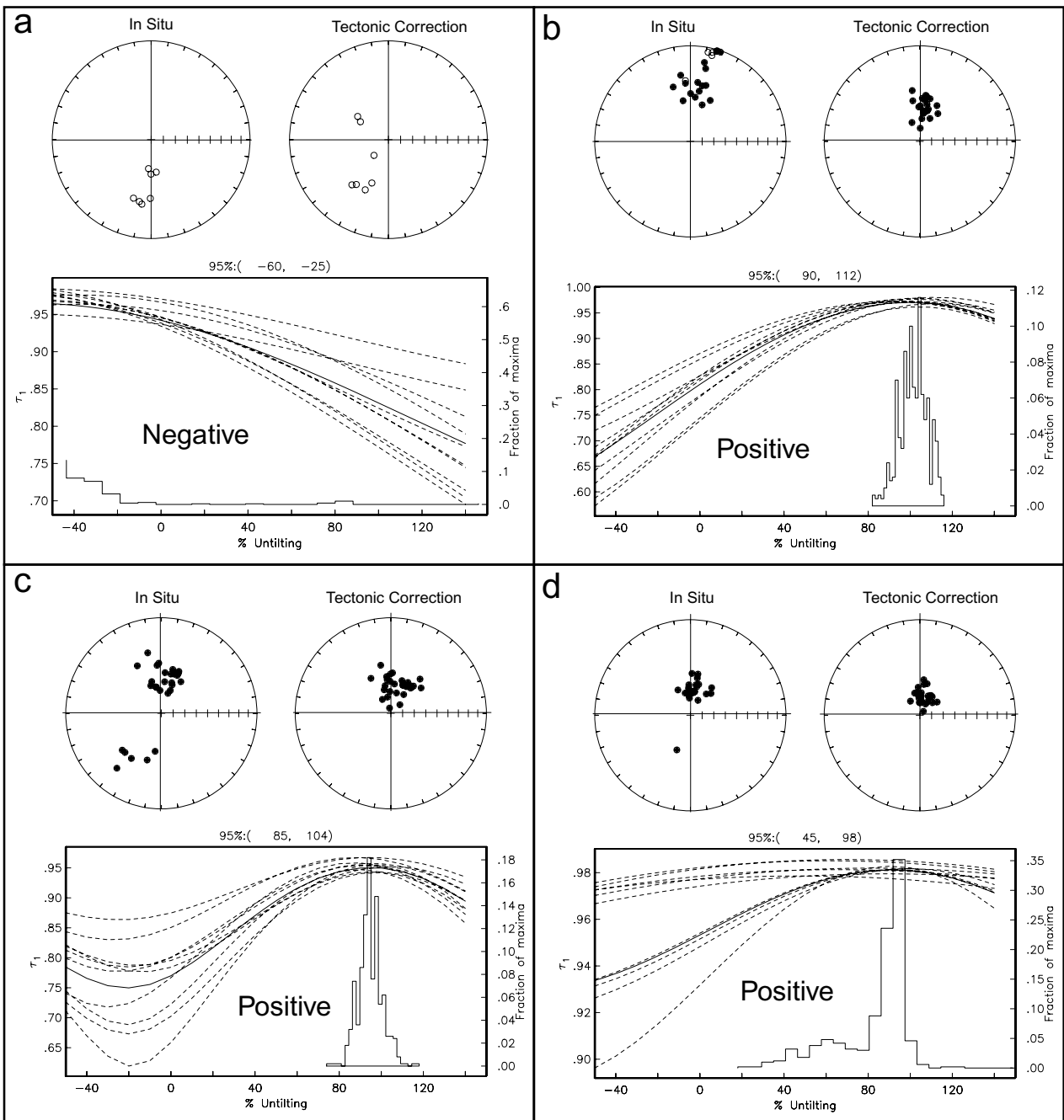


Figure 7. Results of the fold-test of Tauxe & Watson (1994). Equal area projections show site means prior to and after tectonic tilt correction of (a) the lower seven sites of the Jaran Bogd section (negative); (b) the remaining 21 sites of the Jaran Bogd section that pass our selection criteria (see Table 2) (positive); (c) locality SE Baga Bogd (29 sites; positive) and (d) locality SE Artz Bogd (24 sites; positive).

When comparing the declinations and inclinations of our localities with those expected based on the reference paths (Table 7), it is clear again that the SE Artz Bogd locality has a deviating inclination at the 95 per cent confidence level, which is approximately $9 \pm 5^\circ$ steeper than expected for Eurasia. However, the declinations of all localities do not significantly differ from the reference directions. Our analysis, therefore, clearly shows that no vertical axis rotations of more than the confidence limit ($\sim 10^\circ$) have occurred since the early Cretaceous (Table 7).

6 DISCUSSION

6.1 Geochronology and stratigraphy

Our newly obtained $^{40}\text{Ar}/^{39}\text{Ar}$ results for the Bulgantiin Uul section give an age of 124.3 ± 0.9 Ma for sample BU23, which is located approximately 300 m stratigraphically below sample BU56 with an age of 122.7 ± 0.8 Ma (Fig. 2). If sedimentation rates were constant, then the base of the section, which is laterally equivalent to the Baga Bogd locality, would be approximately 126 Ma old. Locality

Table 2. (Continued.)

Locality	Lava/neck site	lat	lon	Type	Na	Nc	q	Tilt		Tilt corrected			In Situ			Tilt Corrected			Age				
								Strike/dip	λ	ϕ	K	A95	palat	D	I	D	ΔD	I		ΔI	k	$\alpha 95$	pol
<i>South-East Baga Bogd</i>																							
<i>Baga Bogd</i>																							
BA I	44.7705	101.8514			36	29	1	090/10	79.9	159.2	18.8	6.3	44.8	351.2	71.1	15.0	8.9	63.3	5.1	408.2	3.8	n	124.7±0.8 to 122.7±0.8 Ma
BA II	44.7693	101.8512			7	5	1	090/10	73.2	180.3		45.5	18.0	54.4	24.0		63.8		108.0	5.8	n		
BA III	44.7686	101.8508			7	6	1	090/10	77.3	32.9		40.6	22.7	50.7	29.0		59.7		103.2	6.6	n		
BA IV	44.7673	101.8502			7	6	1	090/10	84.3	164.7		38.9	354.9	48.3	353.5		58.2		140.1	5.2	n		
BA V	44.7672	101.8416			7	7	1	090/10	76.1	197.4		46.6	5.3	54.8	7.2		64.7		138.1	5.7	n		
BA VI	44.7672	101.8376			7	6	1	090/10	68.7	179.2		41.4	14.6	50.8	18.8		60.4		189.7	4.9	n		
BA VII	44.7673	101.8361			7	6	2	090/10	69.4	262.5		25.0	6.8	33.1	7.8		43.0		21.6	14.8	n		
<i>Bulgantiiin Uul</i>																							
BL I	44.7921	101.9531			7	6	1	073/12	71.2	309.8		28.5	347.3	35.4	348.2		47.4		134.1	5.8	n		
BL II	44.7912	101.9525		gc	7	6	1	073/12	66.0	0.8		35.9	333.2	43.6	330.5		55.4		1303.7	1.9	n		
BL III	44.7905	101.9522			7	6	1	073/12	63.8	185.4		41.8	23.0	52.5	36.3		60.8		330.8	3.7	n		
BL IV	44.7896	101.9507			7	0	3	077/10															
BL V	44.7758	101.9523			7	6	1	077/10	74.3	133.7		57.0	6.0	62.8	15.8		72.0		233.5	4.4	n		
BL VI	44.7741	101.9530			7	5	1	077/10	82.9	-72.3		36.8	357.1	46.4	359.1		57.1		110.0	7.3	n		
BL VII	44.7730	101.9527		gc	7	6	1	077/10	74.1	180.9		45.5	13.9	55.2	22.7		63.8		774.9	2.4	n		
BL VIII	44.7720	101.9536			7	7	1	077/10	56.1	128.9		69.5	18.2	72.1	46.6		79.4		572.6	2.5	n		
BL IX	44.7695	101.9538		gc	7	6	1	090/15	63.5	106.8		71.1	176.8	-70.5	186.5		-80.2		608.7	2.7	r		
BL X	44.7683	101.9539		gc	7	6	1	077/09	70.3	87.1		63.5	168.1	-66.9	168.8		-75.9		1060.5	2.1	r		
BL XI	44.7676	101.9383			7	0	2	094/11															
BL XII	44.7552	102.0059			7	6	1	031/12	51.9	186.3		36.5	31.7	58.1	50.1		56.0		268.3	4.1	n		
BL XIII	44.7538	102.0086			7	5	2	025/13	60.7	175.8		34.7	14.6	53.9	32.7		54.2		39.0	12.4	n		
BL XIV	44.7529	102.0247			7	7	1	030/10	63.1	179.9		44.0	18.7	62.3	38.0		62.6		247.8	3.8	n		
BL XV	44.7539	102.0347			7	7	1	007/11	60.7	186.2		40.4	20.8	64.0	39.8		59.6		356.1	3.2	n		
<i>Bulgantiiin Uul North</i>																							
BN I	44.8096	102.0090			7	6	1	296/70	62.0	182.0		42.4	196.9	47.7	38.8		61.3		93.1	7.0	n		
BN II	44.8170	102.0072		gc	7	5	1	296/70	56.0	200.4		31.8	189.3	56.9	40.5		51.1		713.0	2.9	n		
BN III	44.8172	102.0067		gc	7	6	1	296/70	89.3	106.9		44.0	222.9	43.5	358.8		62.6		182.0	4.5	n		
BN IV	44.8173	102.0059		gc	7	7	1	296/70	84.8	342.6		42.1	226.7	43.2	353.9		61.0		862.7	2.1	n		
BN V	44.8177	102.0046		gc	7	6	1	296/70	64.2	70.2		63.8	219.0	27.0	328.7		76.2		1192.4	1.9	n		
BN VI	44.8179	102.0038		gc	7	6	1	290/80	72.9	188.2		43.4	197.9	37.8	23.6		62.1		255.9	4.2	n		
BN VII	44.8187	102.0019		gc	7	6	1	290/80	80.6	269.9		35.6	213.6	42.8	2.5		55.1		186.1	4.9	n		
<i>Khalzan Khairkhan</i>																							
KK I	44.7208	102.0697			7	7	2	045/05	44.0	77.9		74.1	292.7	77.5	279.4		81.9		15.7	15.7	n		
KK II	44.7204	102.0688		gc	7	5	1	045/05	76.9	56.6		52.8	339.1	64.7	344.4		69.2		182.6	5.7	n		
KK III	44.7199	102.0687			7	6	2	045/05	82.9	59.8		47.9	345.0	61.5	350.5		65.7		30.8	12.3	n		
KK IV	44.7185	102.0680			7	7	1	045/05	65.9	154.2		54.8	21.4	69.1	34.5		70.6		253.9	3.8	n		
KK V	44.7181	102.0682			7	0	3	045/05															
KK VI	44.7185	102.0688			7	7	1	045/05	78.4	95.7		56.1	349.4	67.5	357.7		71.4		221.0	4.1	n		
KK VII	44.7189	102.0695			7	6	1	045/05	81.3	39.7		48.2	343.2	61.6	348.4		65.9		790.1	2.4	n		
<i>Unegr Khairkhan</i>																							
UK I	44.6563	102.1002			7	3	4		-7.1	59.2	52.7	17.2	25.2	73.8	44.5	228.3	19.1	43.3	22.3		n/r	e. Cretaceous	
UK II	44.6574	102.0926		gc	7	0	3	142/40															
UK III	44.6588	102.0914			7	7	2	142/40	16.8	198.3		7.4	254.8	22.6	253.7		-14.6		38.1	9.9	r		
UK IV	44.6839	102.0567		gc	7	6	1	142/40	-6.8	34.1		19.4	238.8	4.6	240.3		-35.1		55.1	9.1	r		
					7	6	1	142/40	-1.1	58.6		29.9	73.5	-88.9	52.6		-49.0		217.8	4.5	r		

Table 2. (Continued.)

Locality	Tilt			Tilt corrected			In Situ			Tilt Corrected			Age								
	lat	lon	Type	Na	Nc	q	Strike/dip	λ	ϕ	K	A95	palat		D	I	ΔD	I	ΔI	k	ϵ_{95}	pol
Lava/neck site																					
UK V	44.6764	102.0583		7	6	1	142/40	-15.3	68.1			22.5	177.9	74.6	215.8	39.7		197.7	4.8	n	
UK VI	44.6753	102.0681	gc	7	6	1	142/40	-4.8	51.1			22.8	253.4	79.5	237.0	40.1		72.9	7.9	n	
UK VII	44.6897	102.0185		7	0	3	120/40	-	-			-	-	-	-	-		-	-	-	
<i>South-East Artz Bogd</i>				26	24	1		75.6	132.3	38.1	4.9	59.2	7.3	69.3	10.3	9.6	73.4	3.0			<i>119.3 ± 0.4 Ma to</i>
<i>Tsagaan Tsav</i>																					<i>115.4 ± 0.4 Ma [1]</i>
TT I	44.4021	102.4217		7	7	1	075/10	85.1	189.4			44.8	2.3	53.9	8.0	63.3		218.7	4.1	n	
TT II	44.4018	102.4221		7	5	1	075/10	63.4	128.0			66.1	9.5	69.1	28.1	77.5		134.7	5.8	n	
TT III	44.4017	102.4221		7	7	2	075/10	56.7	109.2			76.6	321.9	75.2	16.8	83.4		29.5	12.5	n	
TT IV	44.4008	102.4224	gc	7	7	1	075/10	60.7	74.5			62.8	333.9	65.9	326.5	75.6		692.3	2.3	n	
TT V	44.4005	102.4223	gc	7	5	1	075/10	70.2	103.2			65.6	356.3	67.5	4.8	77.2		602.9	3.1	n	
TT VI	44.3927	102.4219		7	5	1	075/10	63.9	140.5			58.9	12.7	65.0	27.9	73.2		123.7	6.0	n	
TT VII	44.3923	102.4212		7	7	1	075/10	68.2	152.1			54.8	15.2	62.6	29.3	70.6		168.4	4.7	n	
TT VIII	44.3913	102.4207	gc	7	7	1	075/10	73.1	111.2			59.4	357.2	63.9	4.2	73.5		374.1	3.1	n	
TT IX	44.3906	102.4211		7	6	1	075/10	70.5	137.6			57.0	10.4	63.5	23.4	72.0		1290.6	1.9	n	
TT X	44.3889	102.4204		7	7	1	075/10	61.6	121.6			69.3	6.9	70.7	26.6	79.3		630.5	2.4	n	
<i>Khatavch</i>																					
KH I	44.3030	102.4035		7	6	1	000/00	75.3	94.0			58.2	-	-	355.4	72.8		108.8	6.5	n	
KH II	44.3023	102.4035		7	6	1	000/00	85.4	73.0			48.3	-	-	356.6	66.0		554.2	2.8	n	
KH III	44.3019	102.4035		7	7	1	000/00	78.3	77.9			54.8	-	-	347.0	70.6		437.6	2.9	n	
KH IV	44.3008	102.4035		7	7	1	000/00	79.7	81.7			55.0	-	-	352.2	70.7		245.3	3.9	n	
KH V	44.2933	102.4038		7	7	1	000/00	72.1	94.9			62.5	-	-	357.0	75.4		292.4	2.7	n	
KH VI	44.2929	102.4038		7	7	1	000/00	79.2	119.0			55.0	-	-	3.8	70.7		756.7	2.2	n	
KH VII	44.2926	102.4030		7	7	1	000/00	78.3	115.2			56.7	-	-	358.6	71.8		294.4	3.5	n	
<i>Kharaat Uul</i>																					
KU I	44.4538	102.6255		7	6	1	110/10	75.7	150.9			69.5	10.6	69.7	2.0	79.4		439.4	3.7	n	
KU II	44.4526	102.6254		7	5	1	110/10	79.0	142.5			68.9	8.3	69.5	357.9	79.1		133.7	6.6	n	
KU III	44.4519	102.6252		7	7	1	110/10	66.0	135.3			81.1	27.0	75.7	42.4	85.5		551.5	2.6	n	
KU IV	44.4514	102.6248		7	7	1	135/11	63.9	188.2			55.4	37.7	60.1	33.8	71.0		624.3	2.4	n	
KU V	44.4504	102.6222		7	6	1	110/08	62.1	167.2			61.5	36.8	67.3	45.1	74.8		431.6	3.2	n	
KU VI	44.4379	102.6208		7	7	1	110/08	61.5	172.6			56.1	43.4	64.3	52.6	71.4		81.1	6.7	n	
KU VII	44.4354	102.6230	gc	7	5	1	125/06	83.7	232.6			40.1	10.5	53.9	6.4	59.3		425.6	3.7	n	
KU VIII	44.4034	102.6097		7	7	1	280/50	78.3	78.7			54.7	201.3	58.1	352.0	70.5		377.9	3.1	n	
KU IX	44.2764	102.7864		7	7	1	085/05	79.8	193.5			43.6	10.6	57.5	13.1	62.3		262.8	3.7	n	
<i>Tsost Magmatic Field</i>				10	7		000/00	82.1	144.9	19.2	14.1	48.6			6.5	21.6	66.2	10.5			<i>107 ± 1.0 Ma to</i>
TS I	44.2884	102.3413		7	5	1	000/00	71.4	159.6			51.5	-	-	25.5	68.3		200.3	5.4	n	
TS II	44.2860	102.3225		7	5	1	000/00	57.1	145.8			60.2	-	-	45.1	74.0		579.5	3.2	n	
TS III	44.2568	102.1693	gc	7	6	1	000/00	71.0	133.5			59.2	-	-	19.3	73.4		660.1	2.6	n	
TS IV	44.2574	102.1842		7	0	2	000/00	-	-			-	-	-	-	-		-	-	-	
TS V	44.2546	102.1861		7	0	2	000/00	-	-			-	-	-	-	-		-	-	-	
TS VI	44.2715	102.2012	gc	7	7	1	000/00	78.2	54.3			51.5	-	-	345.6	68.3		176.1	4.6	n	
TS VII	44.2718	102.2013		7	6	1	000/00	81.1	225.8			38.9	-	-	9.6	58.2		2354.2	1.4	n	
TS VIII	44.2742	102.1927	gc	7	6	1	000/00	69.2	342.3			31.7	-	-	338.8	51.0		1185.2	1.9	n	
TS IX	44.2762	102.1903		7	6	1	000/00	81.4	207.1			41.0	-	-	11.1	60.1		159.4	5.3	n	
TS X	44.2838	102.1895		7	6	4	000/00	27.7	244.8			13.5	-	-	33.9	-25.7		285.0	4.0	r	

Table 2. (Continued.)

Locality	Tilt		Tilt corrected				In Situ				Tilt Corrected				Age									
	lon	lat	Type	Na	Nc	q	Strike/dip	λ	ϕ	K	A95	palat	D	I		D	I	ΔD	I	ΔI	k	$\alpha 95$	pol	
<i>Ariz Bogd [2]</i>																								
95*	102.2825	44.2564	gc	6	3	4	000/00	40.7	59.2	25.5	5.8	49.3	12.0	66.7	278.8	8.9	4.3	67.7	4.3	6721.6	5.4	n	n	
96*	102.2825	44.2564		6	3	1	000/00	63.9	174.4			46.4	37.3	72.9	37.3			64.5		520.7	4.3	n	n	
97*	102.2347	44.2960	gc	6	4	4	000/00	22.5	-163.2			12.4	250.5	-23.7	250.5			-23.7		457.5	6.6	r	n	
98*	102.1994	44.2799		6	6	4	000/00	-11.9	42.9			12.4	59.5	-23.7	59.5			-23.7		59.8	3.6	r	n	
99*	102.1994	44.2799	gc	6	4	4	000/00	-29.5	59.9			6.7	216.2	13.3	216.2			13.3		194.8	5.4	n	n	
100*	102.1994	44.2799		6	6	4	000/00	-22.0	49.4			8.1	228.3	15.8	228.3			15.8		354.8	3.6	n	n	
101*	102.1994	44.2799		6	6	4	000/00	11.9	37.6			26.4	260.6	44.8	260.6			44.8		156.2	3.9	n	n	
102*	102.1787	44.2628		6	4	1	000/00	79.8	-165.6			43.0	14.0	61.8	14.0			61.8		652.3	4.1	n	n	
103*	102.1864	44.2629		6	6	1	000/00	82.2	57.5			49.5	351.5	66.9	351.5			66.9		297.5	3.6	n	n	
104*	102.1864	44.2629		6	5	1	000/00	73.2	66.7			56.8	342.1	71.9	342.1			71.9		353.9	6.5	n	n	
105-106*	102.1895	44.2604		12	11	1	000/00	89.3	70.4			44.8	359.5	63.3	359.5			63.3		160.3	8.9	n	n	
107*	102.1860	44.2596		6	6	1	000/00	65.6	118.9			66.8	17.6	77.9	17.6			77.9		108.5	2.5	n	n	
108*	102.1697	44.2600		6	6	1	000/00	63.2	116.8			69.3	18.8	79.3	18.8			79.3		57.8	6.6	n	n	
109*	102.1697	44.2600		6	5	1	000/00	73.4	-179.8			45.3	23.4	63.7	23.4			63.7		902.6	4.0	n	n	
110*	102.1411	44.2712		6	5	1	000/00	72.1	-157.9			38.8	22.8	58.1	22.8			58.1		134.6	3.7	n	n	
111*	102.1411	44.2712		6	6	1	000/00	83.7	-92.3			38.1	2.0	57.5	2.0			57.5		287.8	5.3	n	n	
112*	102.1411	44.2712		6	5	1	000/00	82.6	-155.7			42.3	9.8	61.2	9.8			61.2		435.0	8.8	n	n	
113*	102.1442	44.2734		4	4	1	000/00	71.7	-35.5			29.8	345.9	48.9	345.9			48.9		304.1	7.8	n	n	
114*	102.1442	44.2734		6	6	1	000/00	79.3	-24.8			37.3	349.2	56.7	349.2			56.7		58.5	8.7	n	n	
115*	102.1444	44.2927		6	5	1	000/00	69.2	167.8			49.3	29.7	66.7	29.7			66.7		96.2	2.9	n	n	
116*	102.1444	44.2927	gc	6	6	1	000/00	79.7	85.3			54.1	354.9	70.1	354.9			70.1		65.2	4.9	n	n	
117-118*	102.1384	44.2826		12	11	1	000/00	63.9	-152.2			32.8	30.3	52.2	30.3			52.2		250.0	4.6	n	n	
119*	102.1305	44.2895		6	6	1	000/00	52.5	164.3			49.3	55.5	66.7	55.5			66.7		189.9	11.6	n	n	
120*	102.0841	44.2837		6	4	1	000/00	64.5	136.1			62.3	31.2	75.3	31.2			75.3		407.2	5.1	n	n	
121*	102.1246	44.2939		6	6	2	000/00	70.7	-136.1			40.6	19.4	51.7	19.4			51.7		34.1	5.2	n	n	
122*	102.1246	44.2939		6	6	1	000/00	72.2	-164.0			40.6	23.7	59.7	23.7			59.7		171.0	3.6	n	n	
123*	102.1223	44.2748	gc	6	4	1	000/00	57.6	94.5			75.8	343.1	82.8	343.1			82.8		429.3	2.6	n	n	
124*	102.1196	44.2723	gc	6	6	1	000/00	81.3	144.2			50.4	9.1	67.5	9.1			67.5		390.9	2.1	n	n	
125*	102.1196	44.2723		4	3	1	000/00	77.1	147.2			52.5	15.0	69.0	15.0			69.0		2172.1	3.7	n	n	
126*	102.1196	44.2723		4	4	1	000/00	80.0	156.9			49.4	12.6	66.8	12.6			66.8		1862.8	10.7	n	n	
127*	102.1196	44.2723		6	6	1	000/00	75.1	122.5			57.9	9.7	72.6	9.7			72.6		335.6		n	n	
128*	102.1196	44.2723		4	4	1	000/00	83.9	-155.2			42.6	8.1	61.5	8.1			61.5		75.3		n	n	
<i>Shovon/Khurmen Uul [2,3]</i>																								
141*	103.7974	44.4542	gc	24	20	1	?	80.8	191.8	31.9	5.9	42.8	12.2	61.6	12.2	8.1	5.0	61.6	5.0	201.7	4.3	n	n	
142-144*	103.7831	44.4457		7	7	1	?	70.0	-69.8			24.5	357.6	42.4	357.6			42.4		177.8	3.3	n	n	
143*	103.7954	44.4420		12	12	1	?	67.4	175.4			47.1	32.4	65.1	32.4			65.1		832.6	3.2	n	n	
145*	103.8144	44.3543		6	4	1	?	67.9	-170.1			41.8	30.3	60.8	30.3			60.8		1146.8	2.7	n	n	
146*	103.8012	44.3554		6	6	1	?	73.0	163.3			50.8	23.5	67.8	23.5			67.8		1579.7	1.7	n	n	
147*	103.7965	44.3795		6	6	1	?	75.9	151.1			52.8	17.2	69.2	17.2			69.2		403.4	3.8	n	n	
148*	103.8042	44.3831		5	5	1	?	61.9	106.6			72.4	4.3	81.0	4.3			81.0		765.1	2.8	n	n	
149*	103.7786	44.3940		6	6	4	?	56.4	31.8			44.8	31.2	63.3	31.2			63.3		323.4	3.7	n	n	
150*	103.7752	44.4057		6	5	1	?	71.1	160.6			52.1	26.1	68.7	26.1			68.7		494.8	3.4	n	n	
151*	103.7895	44.4146		5	4	1	?	76.9	-175.1			45.0	18.5	63.4	18.5			63.4		1234.7	2.6	n	n	

Table 2. (Continued.)

Locality	Lava/neck site	lat	lon	Type	Na	Nc	q	Tilt		Tilt corrected				In Situ				Tilt Corrected				Age	
								Strike/dip	λ	φ	K	A95	palat	D	I	D	ΔD	I	ΔI	k	α95		pol
152*	44.4320	103.8026			5	5	1	?	80.4	-145.1		40.3	-	11.8		59.5	392.2	3.9	n				
153*	44.4402	103.8109		gc	5	5	1	?	75.3	-144.4		37.6	-	17.3		57.0	236.4	5.4	n				
154*	44.4562	103.7884		gc	6	6	1	?	83.8	-120.9		39.9	-	5.7		59.1	125.7	6.0	n				
155*	44.4580	103.7823			4	3	1	?	77.2	-79.3		31.7	-	0.8		51.0	723.3	4.6	n				
156*	44.4568	103.7749		gc	7	5	1	?	78.0	-55.3		33.1	-	354.9		52.5	116.8	7.3	n				
157*	44.4515	103.7702			6	5	1	?	81.0	-53.5		36.0	-	355.7		55.5	288.5	4.5	n				
158*	44.4536	103.7632			6	5	1	?	74.1	-159.4		40.6	-	21.0		59.7	602.9	3.1	n				
159*	44.4554	103.7411		gc	5	4	2	?	-8.3	22.6		0.5	-	257.9		1.0	33.9	16.0	n				
160*	44.4185	103.8107			5	5	1	?	77.1	165.6		49.3	-	17.6		66.7	300.0	4.4	n				
25**	43.9817	102.9869			10	10	1	?	82.0	-102.5		36.7	-	4.3		56.1	154.4	3.9	n				
26-27**	43.9817	102.9869		gc	20	5	1	?	83.7	-136.7		40.6	-	7.2		59.7	209.4	5.3	n				
30**	43.9930	102.9908			8	8	2	?	77.1	119.6		56.2	-	6.6		71.5	46.6	8.2	n				
31-33**	44.0128	102.9892			15	15	2	?	70.4	-13.3		33.2	-	338.9		52.6	39.0	6.2	n				
34**	44.0286	103.0053			10	10	1	?	64.1	-144.7		30.4	-	27.9		49.6	406.1	2.4	n				
<i>Dulaan Bogd Jurassic</i>																							
DR I	44.9253	101.0585			10	8	2		62.9	133.2	2.7	41.8	82.7	182.1	-10.5	75.6	24.8		<i>Jurassic?</i>				
DR II	44.9253	101.0586			7	7	1	095/45	66.8	220.3		30.8	197.0	-6.28	-49.9		205.6	4.2	r				
DR III	44.9250	101.0586			7	6	1	095/75	36.2	138.4		60.7	201.3	-14.1	-74.2		287.2	3.6	r				
DR IV	44.9244	101.0591			7	0	2	095/75	-	-		-	-	-	-	-	-	-	-				
DR V	44.9234	101.0597			7	7	1	095/75	45.0	145.8		58.9	200.9	-8.35	-73.1		710.1	2.3	r				
DR VI	44.9232	101.0599			7	7	1	095/75	10.9	150.3		35.5	41.2	22.76	55.0		110.9	5.8	n				
DR VII	44.9230	101.0670			7	7	1	055/55	0.1	163.5		19.2	45.2	61.61	34.8		385.9	3.1	n				
DR VIII	44.9230	101.0673			7	6	1	060/70	43.3	2.6		24.5	134.3	25.2	-42.3		127.0	6.0	r				
DR IX	44.9229	101.0678			7	6	1	060/70	67.6	39.3		50.8	149.8	2.299	-67.7		51.6	9.4	r				
DR X	44.9226	101.0684			7	6	1	070/65	53.7	7.8		33.1	145.0	9.645	-52.4		298.5	3.9	r				
					7	6	2	070/65	37.2	1.4		19.2	129.0	21.12	-34.9		19.5	15.6	r				

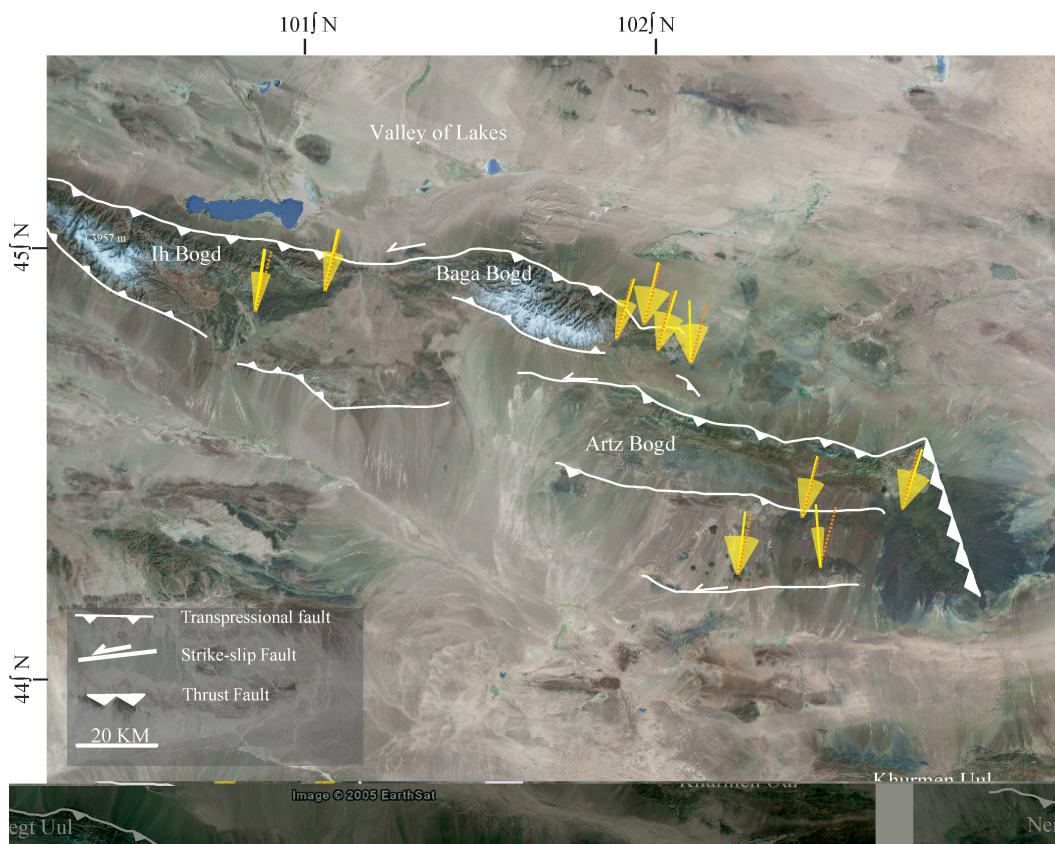


Figure 8. Map of the NE Gobi Altai with the declinations of our newly sampled sites, and error bars (both in yellow). The reference declination based on the Apparent Polar Wander Paths of stable Eurasia of Besse & Courtillot (2002), Schettino & Scotese (2005) and Torsvik *et al.* (in press) ($\sim 15^\circ$ for the period between 130 and 120 Ma and $\sim 12^\circ$ for the period 100–90 Ma, see Table 5) are indicated as dotted orange line.

Khalzan Khairkhan occurs at the top of the stratigraphic section and its age is probably about 120 Ma or slightly older. A comparable time-span may also represent the Tsagaan Tsav and Khataavch sections where approximately 750 m of lavas and sediments were deposited between 119.3 ± 0.4 and 115.4 ± 0.4 Ma (Barry 1999). In the Jaran Bogd section, sample JB57 with an age of 124.7 ± 0.8 Ma was taken approximately 400 m below sample JB94 (121.9 ± 0.8 Ma), which was collected near the top of the section. Again, comparable sedimentation rates are calculated. However, sample JB26 was sampled approximately 400 m stratigraphically below JB57, yet gives an age of 118.2 ± 0.8 Ma, significantly younger than the higher samples. We therefore, conclude that this sample was obtained from a younger sill. However, because since the majority of the samples we collected were obtained from basalts with clear extrusive characteristics such as upward increasing vesicularity, pahoehoe structures or occasionally pillows, the palaeomagnetic results obtained from this section are representative for the ~ 125 –122 interval or slightly older. Assuming a constant sedimentation rate, the base of the section would be approximately 129 Ma old.

6.2 Anomalous inclination at Artz Bogd

As clearly shown in our statistical analyses, locality Artz Bogd yields a significantly steeper inclination than both the older and younger localities, as well as the three reference paths (Tables 6 and 7). This may be explained by (1) insufficient averaging of secular variation, by chance leading to an anomalously steep inclination, (2) overcorrection of bedding tilt or (3) palaeolatitudinal drift.

To test whether secular variation is averaged out, we compare the scatter of directions in our localities with the expected scatter at the palaeolatitude of Mongolia in the interval of 110–80 Ma of McFadden *et al.* (1991; Table 8). The scatter in the combined Ih Bogd/Baga Bogd locality, the combined Tsost/Shovon/Khurmen Uul locality and the combined Cretaceous data set do not significantly differ from the expected scatter is $S\lambda = 16.9$ ($S\lambda = 14.9$, $Su = 19.5$), whereas the scatter in the SE Artz Bogd locality is significantly lower: $S\lambda = 14.0$ ($S\lambda = 11.5$, $Su = 16.0$). Even though 24 lavas were averaged, the low scatter shows that secular variation is not averaged out. This may be caused by a very rapid outflow of lavas, such that a series of consecutive lavas represent the same spot reading of the Earth's magnetic field influencing the average. We tested this for the seven lavas of Khataavch, which together yield a κ -value of 241, much higher than expected in a secular variation scatter (which has a k -value of typically 20–50 for directions (Tauxe & Kent 2004), which corresponds to a κ of 10–30 for the poles). However, none of the lavas in Khataavch share a common true mean direction with the next or previous one, showing that each direction obtained from this section is a separate spot reading, which by chance happen to cluster tightly.

An important point of discussion before one can conclude palaeolatitudinal drift from palaeomagnetic directions of lavas is the issue of tilt correction. As stated earlier, we choose to correct for bedding tilt, because we obtain positive fold tests and the region has tilted Tertiary peneplains and tilted fine-grained sediments, which proves that the majority of the tilt is post-depositional. However, the early Cretaceous basin configuration concluded from sedimentological

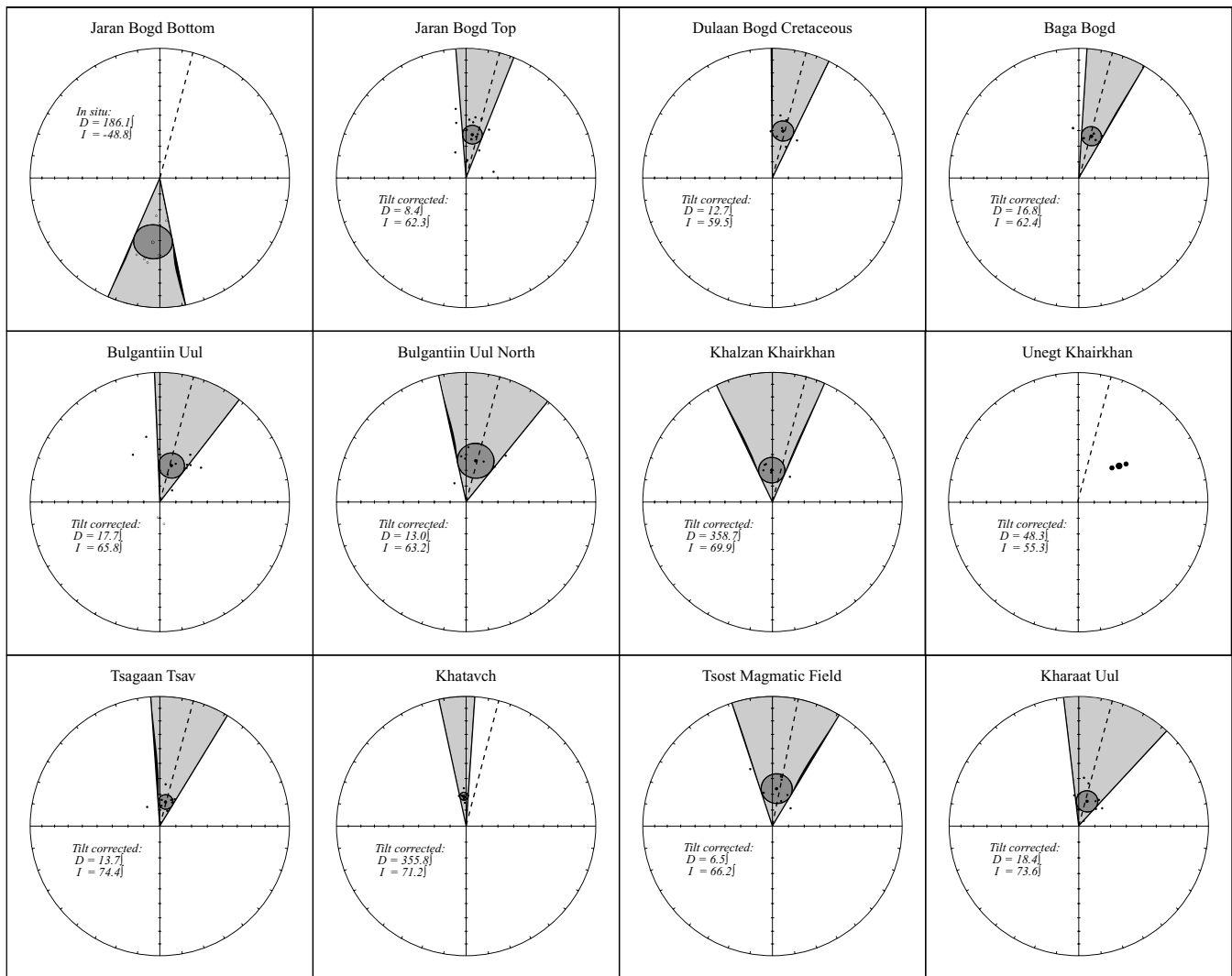


Figure 9. Equal area projections of the main sampling localities, indicating our average directions, as well as the reference declination based on the Apparent Polar Wander Paths of stable Eurasia of Besse & Courtillot (2002), Schettino & Scotese (2005) and Torsvik *et al.* (in press), indicated by the dotted line. D = declination, I = inclination.

Table 3. Common true mean direction tests using statistics of McFadden & Lowes (1981) for five localities. The results show that there is a statistically significant difference at 95 per cent confidence between the 124–118 Ma, 119–115 Ma and 105–92 Ma groups. γ = angle between the two data sets; γ_c = critical angle.

Groups	γ	γ_c	Classification
SE Ih Bogd (124–118 Ma) vs SE Baga Bogd (125–122 Ma)	5.3	5.9	B
Ih & Baga Bogd (125–118) vs SE Artz Bogd (119–115 Ma)	8.4	4.4	NEG
Tsost Field (107–94 Ma) vs Shovon & Khurmen Uul (94–92 Ma)	0.5	5.2	B
SE Artz Bogd (119–115 Ma) vs Tsost/Shov./Khur.U. (107–92 Ma)	8.7	4.1	NEG
Ih & Baga Bogd (125–118) vs Tsost/Shov./Khur.U. (107–92 Ma)	8.7	4.1	B

Table 4. Average poles and palaeomagnetic directions for the various localities. For key, see Table 2.

Locality	Age	n	λ	ϕ	κ	A95	Palat	D	ΔD	I	ΔI
Ih Bogd & Baga Bogd	125–118 Ma	50	82.0	172.3	22.8	4.3	43.5	11.7	5.9	62.2	3.6
Eastern Artz Bogd	119–115 Ma	24	75.6	132.3	38.1	4.9	59.2	10.3	9.6	73.4	3.0
Tsost Field/Shovon/Khurmen Uul*	105–92 Ma	52	81.1	165.7	26.4	3.9	46.6	11.4	5.7	64.7	3.0
All Cretaceous sites	124–92 Ma	126	80.8	158.4	25.3	2.5	48.2	11.1	3.8	65.9	1.9

Table 5. Poles and directions for the Gobi Altai (44.5°N, 101°E), as predicted by the apparent polar wander paths constructed for stable Eurasia by Besse & Courtillot (2002), Schettino & Scotese (2005) and Torsvik *et al.* (in press) for 90, 100, 110, 120 and 130 Ma. For key, see Table 2.

Locality	Age	<i>n</i>	λ	ϕ	<i>k</i>	$\alpha 95$	Palat	<i>D</i>	ΔD	<i>I</i>	ΔI
Torsvik <i>et al.</i> (in press)	90	27	80.3	169.1	115.2	2.6	47.5	13.3	3.9	65.4	2.0
	100	11	81.0	166.2	125.0	4.1	47.8	12.1	6.1	65.6	3.1
	110	16	80.7	191.4	106.0	3.6	43.9	13.0	5.0	62.5	3.0
	120	24	78.4	196.5	130.5	2.6	42.5	15.8	3.5	61.4	2.2
	130	18	75.2	193.6	143.1	2.9	42.3	20.2	3.9	61.2	2.5
Schettino & Scotese (2005)	90		80.3	174.9		3.4	46.6	13.5	5.0	64.7	2.6
	100		80.8	174.9		5.7	46.5	12.8	8.3	64.6	4.4
	110		80.7	180.4		9.4	45.6	13.1	13.5	63.9	7.4
	120		79.9	186.2		5.0	44.6	14.2	7.0	63.1	4.0
	130		78.4	187.8		9.6	44.2	16.2	13.5	62.8	7.8
Besse & Courtillot (2002)	90	13	82.2	202.1	65.2	5.2	42.6	10.5	7.1	61.5	4.4
	100	12	81.7	180.1	43.0	6.7	45.6	11.7	9.6	63.9	5.3
	110	17	80.0	183.6	74.8	4.2	45.1	14.1	6.0	63.5	3.4
	120	20	78.2	189.4	182.9	2.4	43.8	16.5	3.3	62.5	2.0
	130	14	75.8	192.9	205.5	2.8	42.6	19.5	3.8	61.5	2.4

Table 6. Results of a common true mean direction test between the reference pole points of Besse & Courtillot (2002), Schettino & Scotese (2005) and Torsvik *et al.* (in press) for 90, 100, 110, 120 and 130 Ma and the results of our localities, using the method of McFadden & Lowes (1981).

	130 Ma	120 Ma	110 Ma	100 Ma	90 Ma
Torsvik <i>et al.</i> (in press)					
Ih & Baga Bogd (124–118)	NEG	A	B	B	B
SE Artz Bogd (119–115 Ma)	NEG	NEG	NEG	NEG	NEG
Tsost/Sh./K.U. (105–92 Ma)	NEG	NEG	B	B	A
All sites (124–92 Ma)	NEG	NEG	NEG	A	A
Schettino & Scotese (2005)					
Ih & Baga Bogd (124–118)	B	B	B	B	B
SE Artz Bogd (119–115 Ma)	NEG	NEG	NEG	NEG	NEG
Tsost/Sh./K.U. (105–92 Ma)	B	B	B	B	A
All sites (124–92 Ma)	NEG	NEG	A	A	A
Besse & Courtillot (2002)					
Ih & Baga Bogd (124–118)	NEG	B	B	B	B
SE Artz Bogd (119–115 Ma)	NEG	NEG	NEG	NEG	NEG
Tsost/Sh./K.U. (105–92 Ma)	NEG	NEG	B	B	B
All sites (124–92 Ma)	NEG	NEG	A	B	NEG

observations indicates that all our samples were collected from northern, southward dipping slopes of the basins, which may, therefore, lead to an overcorrection to the north of a few degrees. Moreover, this overcorrection is not necessarily consistent and the original tilt of the lavas may vary locally due to eruption and deposition over slightly uneven topography. Hankard *et al.* (2007b) also addressed this issue. In their earlier paper, Hankard *et al.* (2005) interpreted an anomalously shallow inclination from the six lavas at Khurmen Uul of 10° and suggested palaeolatitudinal drift as the explanation. In their later paper, Hankard *et al.* (2007b) argued that this inclination anomaly may have been caused by correction of ~10° southward bedding tilt at Khurmen Uul, and chose in their re-analysis not to correct for bedding tilt, which led to no significant deviation from the Besse & Courtillot (2002) reference path of Eurasia. In most cases, one can argue for and against bedding tilt, and in this case, one should allow an extra uncertainty of at least a few degrees, and maybe as much as 10° for which interpreting the palaeo-inclination. Especially in the case reported here, where the early Cretaceous basin configuration implies a consistent tilt direction, which prevents averaging out of this error. In conclusion,

we do not interpret the anomalously steep inclination in terms of palaeolatitudinal drift, because insufficient averaging of the secular variation, and small bedding tilt errors may explain the anomaly. However, because we showed that the lavas do represent individual spot readings of the Earth's magnetic field, we integrate all our results of the lower Cretaceous lavas and construct a pole, or rather, an apparent polar wander path without significant plate motion from ~125 to 95 Ma, with $n = 126$, $\lambda = 80.8$, $\phi = 158.4$, $\kappa = 25.3$, $A95 = 2.5$, palaeo-latitude = 48.2 with a scatter $S\lambda = 16.7$ ($SI = 15.3$, $Su = 17.8$) and a regionally consistent direction for the Gobi Altai of $D/I = 11.1/65.9$, $\Delta D/\Delta I = 3.8/1.9$. This is one of the statistically best-determined palaeopoles/APWP's for Asia.

6.3 Tectonic implications

In their study of terminations of strike-slip faults, Bayasgalan *et al.* (1999) suggested a scenario for the formation of the Ih Bogd, Baga Bogd and Artz Bogd restraining bends in which clockwise rotation of the mountain ranges was accommodated by their bounding

Table 7. Differences between our results and the reference pole points of Besse & Courtillot (2002), Schettino & Scotese (2005) and Torsvik *et al.* (in press) for 90, 100, 110, 120 and 130 Ma and the results of our localities in terms of differences in declination and inclination. Rot = rotation calculated by $\text{Declination}_{\text{locality}} - \text{Declination}_{\text{reference}}$, $\Delta\text{rot} = \text{error on rotation}$, calculated by $\sqrt{(\Delta D_{\text{loc}}^2 + \Delta D_{\text{ref}}^2)}$, Dif = difference in inclination calculated by $I_{\text{loc}} - I_{\text{ref}}$, $\Delta\text{inc} = \text{error in inclination difference}$, calculated by $(\Delta I_{\text{loc}}^2 + \Delta I_{\text{ref}}^2)$. For values of $D, I, \Delta D$ and ΔI , see Tables 4 and 5, respectively.

	Declination												Inclination																											
	130				120				110				100				90				130				120				110				100				90			
	rot	Δrot	rot	Δrot	rot	Δrot	rot	Δrot	rot	Δrot	rot	Δrot	rot	Δrot	rot	Δrot	rot	Δrot	rot	Δrot	dif	Δinc	dif	Δinc	dif	Δinc	dif	Δinc	dif	Δinc	dif	Δinc	dif	Δinc	dif	Δinc				
Torsvik <i>et al.</i> (in press)																																								
Ih Bogd & Baga Bogd	-1.6	7.1	-0.4	8.5	-1.8	11.4	-2.7	10.8	-1.6	7.6	-4.4	6.7	-8.8	6.9	-3.2	4.1	-3.4	4.8	7.8	4.3	10.9	4.2	-3.2	4.1	-3.4	4.8	7.8	4.3	10.9	4.2	-3.2	4.1	-3.4	4.8	7.8	4.3	10.9	4.2		
Eastern Artz Bogd																																								
Tsost Field/Shovon/Kh. Uul*	-2.2	5.4	-1.0	7.2	-1.9	6.3	-4.7	5.2	-9.1	5.4	0.5	2.8	0.3	3.6	3.4	3.6	3.4	3.6	3.4	3.6	3.4	3.6	3.4	3.6	3.4	3.6	3.4	3.6	3.4	3.6	3.4	3.6	3.4	3.6	3.4	3.6	3.4	3.6		
All Cretaceous sites																																								
Schettino & Scotese (2005)																																								
Ih Bogd & Baga Bogd	-1.8	7.7	-1.1	10.2	-2.8	16.6	-1.7	14.7	-4.8	14.7	-2.5	4.4	-2.4	5.7	8.8	5.3	9.5	8.0	0.8	8.0	2.4	7.6	-2.5	4.4	-2.4	5.7	8.8	5.3	9.5	8.0	0.8	8.0	2.4	7.6	1.6	5.0	1.9	8.4		
Eastern Artz Bogd																																								
Tsost Field/Shovon/Kh. Uul*	0.6	6.3	-0.6	9.1	-3.0	14.0	-5.4	8.0	-8.4	14.0	4.4	3.2	2.0	4.8	4.4	3.2	2.0	4.8	4.4	3.2	2.0	4.8	4.4	3.2	2.0	4.8	4.4	3.2	2.0	4.8	4.4	3.2	2.0	4.8	4.4	3.2	2.0	4.8		
All Cretaceous sites																																								
Besse & Courtillot (2002)																																								
Ih Bogd & Baga Bogd	1.2	9.2	0.0	11.3	-3.8	11.3	-5.1	6.6	-8.1	6.9	0.7	5.7	-1.7	6.4	9.5	6.1	9.9	4.5	1.2	4.5	2.4	3.9	0.7	5.7	-1.7	6.4	9.5	6.1	9.9	4.5	1.2	4.5	2.2	3.6	3.2	3.8				
Eastern Artz Bogd																																								
Tsost Field/Shovon/Kh. Uul*	0.6	8.1	-0.6	10.3	-3.0	7.1	-5.4	5.0	-8.4	5.4	4.4	4.8	2.0	5.6	4.4	4.8	2.0	5.6	4.4	4.8	2.0	5.6	4.4	4.8	2.0	5.6	4.4	4.8	2.0	5.6	4.4	4.8	2.0	5.6	4.4	4.8	2.0	5.6		
All Cretaceous sites																																								

Table 8. Scatter of poles for the various localities in the Gobi Altai, and for the 110–80 Ma reference interval according to McFadden *et al.* (1991), using statistics of Vandamme (1994).

Locality	<i>n</i>	Sλ	SI	Su
McFadden <i>et al.</i> (1991) 110–80 Ma		16.9	14.9	19.5
Ih Bogd & Baga Bogd	50	16.8	14.4	18.9
Eastern Artz Bogd	24	14.0	11.5	16.0
Tsost Field/Shovon/Khurmen Uul*	52	16.0	13.7	17.9
All Cretaceous sites	126	16.7	15.3	17.8

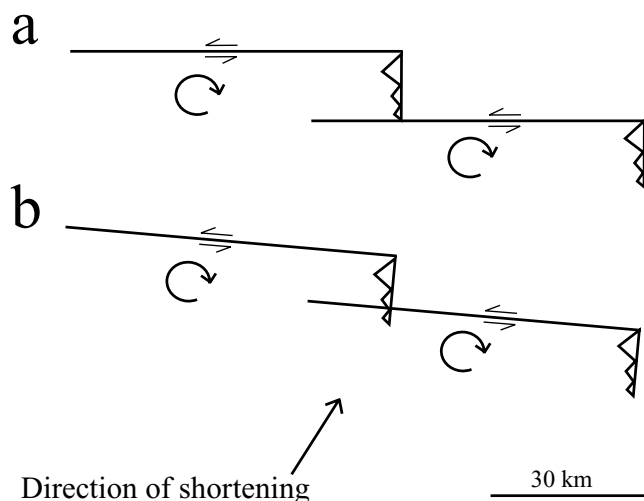


Figure 10. Cartoon illustrating the scenario of rotation at strike-slip zone termination of Bayasgalan *et al.* (1999) leading to thrusting and transpression at the edges of rotating restraining bends (a) prior to and (b) after rotation. Our data indicate that $>10^\circ$ rotations do not occur in the Gobi Altai.

left-lateral strike-slip faults (Fig. 10). Also, Cunningham (2005) discussed the possibility of vertical axis rotation of strike-slip faults to create an increasing component of thrusting during progressive transpressional deformation, as is suggested in the northern Altai by a palaeomagnetic study of the Zaisan basin indicating a Neogene 40° clockwise rotation (Thomas *et al.* 2002). The angle between the transpressional faults and the strike-slip faults in the NE Gobi Altai at present is $20\text{--}30^\circ$, and the absence of rotations larger than our error bar of $\sim 10^\circ$ shows that vertical axis rotations have not played a significant role in the formation of the Ih Bogd, Baga Bogd and Artz Bogd restraining bends in the NE Gobi Altai.

On a large scale, Schlupp (1996) suggested a model in which maximum SW-NE shortening at the junction between the Gobi Altai and Altai mountains, decreasing east and northwest, respectively, would lead to opposite rotation of the strike-slip faults of the Gobi Altai and western Altai (Fig. 11). Our error margin of $\sim 10^\circ$ and a E-W width of the Gobi Altai of approximately 600 km allows a shortening of ~ 100 km at the junction that would remain undetectable for our palaeomagnetic analysis, which would mean that the suggestion of Schlupp (1996) may be valid for the Gobi Altai region (although we note that the Altai widens to the NW and has accommodated more shortening there, not less and appears, therefore, inconsistent with scenario of Schlupp (1996). However, the presence of segments of pure strike-slip without transpression between the restraining bends in the Gobi Altai indicates that it is unlikely that this scenario is of great importance. The presence of these pure strike-slip segments is not demonstrated in this paper. Indeed they appear to be subordinate and less important than the thrusts in Fig. 1.

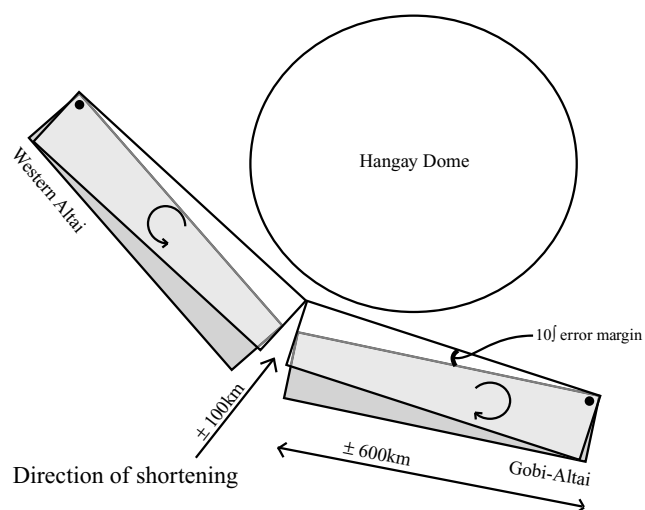


Figure 11. Schematic representation of the scenario of Schlupp (1996), in which opposite rotations in the Western Altai and Gobi Altai accommodate maximum convergence at their junction and no convergence at their north-western and eastern limits, respectively. Our 95 per cent confidence limit of $\sim 10^\circ$ allows 100 km of shortening to be undetectable through palaeomagnetic analysis. The presence of pure strike-slip segments in the NE Gobi Altai suggests that this mechanism is too simplistic.

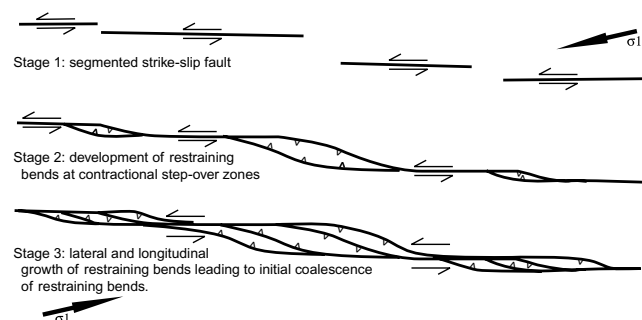


Figure 12. Mechanism by which restraining bends along a right-stepping, left-lateral, strike-slip fault system form, grow and coalesce with time in the NE Gobi Altai, without vertical axis rotations. Modified after Cunningham *et al.* (1996a).

The absence of $>10^\circ$ vertical axis rotations during transpressional mountain building has important implications for the mechanics and kinematics deformation in the NE Gobi Altai. First, we conclude that the restraining bends are thrust-bound ranges that grew in their present orientation. They may have formed between linked en echelon strike-slip segments, or be the result of strain partitioning into pure strike-slip and compressional segments (Fig. 12). Both cases have been documented in Mongolia and elsewhere (Cunningham *et al.* 1996a, 2003a,b; Cunningham 2005; Mann 2007). Restraining bend border thrusts in the Gobi Altai trend subparallel to the pre-Mesozoic basement grain, thus they probably reactivate pre-existing weak zones such as prevailing metamorphic fabric, older faults and lithological boundaries. Conversely, the strike-slip segments crosscut the pre-existing basement grain and are probably newly formed in the late Cenozoic. We suggest that as restraining bends have grown outwards through time, linking E-W strike-slip faults have either persisted and grown in length, or developed components of oblique-slip displacements at their tips where they link with NW-striking thrusts (and thus the pure strike-slip segments have shortened), or the early formed strike-slip faults have

been locally abandoned as new master faults evolve within a strike-slip duplex (although this has not been observed, more structural mapping is needed to test this idea). The implication is that if the strike-slip faults have persisted without rotating, then they must be parallel to the regional slip vector. We note that GPS vectors for the northeast Gobi Altai region are consistent with this interpretation (Calais *et al.* 2003).

Secondly, absence of vertical axis rotations also shows that drag folding, which would cause counter-clockwise vertical axis rotation adjacent to left-lateral faults, has not played a significant role during motion along the Bogd strike-slip zone, even though we have sampled very close to the main fault zones (e.g. Dulaan Bogd Cretaceous, Bulgantiin Uul, Bulgantiin Uul North and Tsagaan Tsav were sampled within hundreds of metres of the main strike-slip faults). From this we infer that the Bogd strike-slip faults are weak, and that strike-slip displacements are not distributed, but localized along the faults. As a consequence, estimates of cumulative strike-slip displacements along different strike-slip faults is likely a good measure for the entire E-W left-lateral displacement associated with late Cenozoic transpressional orogeny in the NW Gobi Altai.

7 CONCLUSIONS

To test the vertical axis rotation history associated with transpressional mountain building, we have carried out a palaeomagnetic study in the NE Gobi Altai mountains of southern Mongolia. We sampled lower Cretaceous lavas, which are widely exposed and allow comparison of rotation histories of the Ih Bogd, Baga Bogd and Artz Bogd restraining bends at the eastern termination of the Bogd strike-slip zone. Our conclusions can be summarized as follows:

1. We provide new $^{40}\text{Ar}/^{39}\text{Ar}$ ages to show that the stratigraphy of mafic lavas and fluvio-lacustrine sediments on the southern flanks of Mt Ih Bogd and Mt Baga Bogd have ages between ~ 125 and ~ 122 Ma, with a sill of ~ 118 Ma old. The lavas are older than previously dated lavas south of Artz Bogd, with ages of 119–115 Ma.
2. Palaeomagnetic results from the 119 to 115 Ma lavas south of Artz Bogd show a significant steeper inclination than both the 125–122 Ma lavas of Baga Bogd and Ih Bogd, as well as the younger lavas and necks newly sampled and previously published from the 107 to 92 Ma Tsost Magmatic Field and Shovon and Khurmen Uul localities. We explain this result by insufficient averaging of secular variation and small errors induced by overcorrection of bedding tilt. We show that individual lavas in the SE Artz Bogd locality represent individual spot readings of the Earth's magnetic field and integrate all results obtained from lower Cretaceous lavas in the Gobi Altai.
3. We present a pole, or rather, an apparent polar wander path without significant plate motion from ~ 125 to 95 Ma, with $n = 126$, $\lambda = 80.8$, $\phi = 158.4$, $\kappa = 25.3$, $A95 = 2.5$, palaeolatitude = 48.2 with a scatter $S\lambda = 16.7$ ($SI = 15.3$, $Su = 17.8$) and a regionally consistent direction for the Gobi Altai of $D/I = 11.1/65.9$, $\Delta D/\Delta I = 3.8/1.9$. This is one of the best-determined palaeopoles/APWP's for Asia.
4. There is no significant deviation of the 125–95 Ma pole position of the Gobi Altai from the reference positions of Eurasia.
5. Formation of the Ih Bogd, Baga Bogd and Artz Bogd restraining bends was not associated with vertical axis rotations larger than our error margin of $\sim 10^\circ$.
6. The Bogd strike-slip zone is a weak fault zone, in which shear is localized.

7. Transpressional deformation in the uplifted ranges of the northeastern Gobi Altai could have developed by linked, but partitioned oblique-thrust and strike-slip fault displacements. Both strike-slip and oblique thrust displacements could follow the regional slip vector without requiring vertical axis rotations.

ACKNOWLEDGMENTS

This research was supported by UK NERC Grant NER/D/S/2003/00671. This paper benefited from reviews of Randy Enkin and an anonymous reviewer. We thank Kishigsuren Sodnom for her help in organizing our 2005 field campaign. Cor Langereis and Guillaume Dupont-Nivet are thanked for discussion. The field crew Uyanga, Butemj, Kheegie, Erkaa and Baadama are thanked for their assistance and company. DJJvH acknowledges an E.J. Garwood grant of the Geological Society of London. GBS was supported by the Molengraaff Foundation and the KF Hein Foundation. Mineral separation facilities were provided by Roel van Elsas, Vrije Universiteit Amsterdam.

REFERENCES

- Badarch, G., Cunningham, W.D. & Windley, B.F., 2002. A new terrane subdivision for Mongolia: implications for the Phanerozoic crustal growth of Central Asia, *J. Asian Earth Sci.*, **21**, 87–110.
- Baljinnyam, I. *et al.*, 1993. Ruptures of major earthquakes and active deformation in Mongolia and its surroundings, *Geol. Soc. Am. Mem.*, **181**, 61pp.
- Barry, T.L., 1999. *Origins of Cenozoic Basalts in Mongolia: A Chemical and Isotope Study*, University of Leicester, Leicester.
- Barry, T.L. & Kent, R.W., 1998. Cenozoic magmatism in Mongolia and the origin of central and east Asian basalts, *Geodynamics*, **27**, 347–364.
- Barry, T.L., Saunders, A.D., Kempton, P.D., Windley, B.F., Pringle, M.S., Dorjnamjaa, D. & Saandar, S., 2003. Petrogenesis of Cenozoic Basalts from Mongolia: evidence for the role of asthenospheric versus metasomatized lithospheric mantle sources, *J. Petrol.*, **44**, 55–91.
- Bayarsayhan, C., Bayasgalan, A., Enhtuvshin, B., Hudnut, K., Kurushin, R.A., Molnar, P. & Ölziybat, M., 1996. 1957 Gobi-Altay, Mongolia, earthquake as a prototype for southern California's most devastating earthquake, *Geology*, **24**, 579–582.
- Bayasgalan, A., Jackson, J., Ritz, J.-F. & Carretier, S., 1999. Field examples of strike-slip fault terminations in Mongolia and their tectonic significance, *Tectonics*, **18**, 394–411.
- Berkey, C.P. & Morris, K.K., 1927. *Geology of Mongolia*, pp. 475, American Museum of Natural History, New York.
- Besse, J. & Courtillot, V., 2002. Apparent and true polar wander and the geometry of the geomagnetic field over the last 200 Myr, *J. geophys. Res.*, **107**, 2300, doi:10.1029/2000JB000050.
- Buchan, C., Cunningham, W.D., Windley, B.F. & Tomurhuu, D., 2001. Structural and lithological characteristics of the Bayankhongor ophiolite zone, Central Mongolia, *J. Geol. Soc. Lond.*, **158**.
- Buchan, C., Pfänder, J., Kröner, A., Brewer, T.S., Tomurtoogoo, O., Tomurhuu, D., Cunningham, W.D. & Windley, B.F., 2002. Timing of accretion and collisional deformation in the Central Asian Orogenic Belt: implications of granite geochronology in the Bayankhongor Ophiolite zone, *Chem. Geol.*, **192**, 23–45.
- Butler, R.F., 1992. *Paleomagnetism: Magnetic Domains to Geologic Terranes*, pp. 195, Blackwell Scientific Publications, Boston.
- Calais, E., Cernolle, M., San'kov, V., Lukhnev, A., Miroshnichenko, A., Amarjargal, S. & Déverchère, J., 2003. GPS measurements of crustal deformation in the Baikal-Mongolia area (1994–2002): implications for current kinematics of Asia, *J. Geophys. Res.*, **108**, ETG 14-1–ETG 14-13.
- Carretier, S., Lucazeau, F. & Ritz, J.-F., 1998. Numerical approach of the interactions between active fault, climate and erosion. Example of the

- Bogd fault, Gobi Altai, Mongolia, *Comptes Rendus de l'Academie des Sciences – Series IIA – Earth planet. Sci.*, **326**, 391–397.
- Carretier, S., Ritz, J.-F., Jackson, J. & Bayasgalan, A., 2002. Morphological dating of cumulative reverse fault scarps: examples from the Gurvan Bogd fault system, Mongolia, *Geophys. J. Int.*, **148**, 256–277.
- Cobbold, P.R. & Davy, P., 1988. Indentation tectonics in nature and experiments. 2. central Asia, *Bull. Geol. Institut. Uppsala*, **14**, 143–162.
- Cogné, J.-P., Kravchinsky, V.A., Halim, N. & Hankard, F., 2005. Late Jurassic–Early Cretaceous closure of the Mongol–Lkhotsk Ocean demonstrated by new Mesozoic palaeomagnetic results from the Trans-Baikal area (SE Siberia), *Geophys. J. Int.*, **163**, 813–832.
- Cox, A., 1969. Research note: confidence limits for the precision parameter, K, *Geophys. J. Roy. Astron. Soc.*, **17**, 545–549.
- Cunningham, W.D., 1998. Lithospheric controls on late Cenozoic construction of the Mongolian Altai, *Tectonics*, **17**, 891–902.
- Cunningham, W.D., 2001. Cenozoic normal faulting and regional doming in the southern Hangay region, Central Mongolia: implications for the origin of the Baikal rift province, *Tectonophysics*, **331**, 389–411.
- Cunningham, W.D., 2005. Active intracontinental transpressional mountain building in the Mongolian Altai: defining a new class of orogen, *Earth planet. Sci. Lett.*, **240**, 436–444.
- Cunningham, W.D., Windley, B.F., Dornjnamjaa, D., Badamgarav, D. & Saander, M., 1996a. Late Cenozoic transpression in southwestern Mongolia and the Gobi–Altai – Tien Shan connection, *Earth planet. Sci. Lett.*, **140**, 67–81.
- Cunningham, W.D., Windley, B.F., Dornjnamjaa, D., Badamgarav, D. & Saander, M., 1996b. A structural transect across the Mongolian Western Altai: active transpressional mountain building in Central Asia, *Tectonics*, **15**, 142–156.
- Cunningham, W.D., Windley, B.F., Owen, L.A., Barry, T., Dornjnamjaa, D. & Badamgarav, J., 1997. Geometry and style of partitioned deformation within a late Cenozoic transpressional zone in the eastern Gobi Altai Mountains, Mongolia, *Tectonophysics*, **277**, 285–306.
- Cunningham, W.D., Davies, S.J. & Badarch, G., 2003a. Crustal architecture and active growth of the Sutai Range, western Mongolia: a major intracontinental, intraplate restraining bend, *J. Geodyn.*, **36**, 169–191.
- Cunningham, W.D., Dijkstra, A.H., Howard, J.P., Quarles, A. & Badarch, G., 2003b. Active intraplate strike-slip faulting and transpressional uplift in the Mongolian Altai, *Special Publication of the Geol. Soc. Lond.*, **210**, 65–87.
- Dankers, P.H.M. & Zijdeveld, J.D.A., 1981. Alternating field demagnetization of rocks, and the problem of gyromagnetic remanence, *Earth planet. Sci. Lett.*, **53**, 89–92.
- Day, R., Fuller, M. & Schmidt, V.A., 1977. Hysteresis properties of titanomagnetites: grain-size and compositional dependence, *Phys. Earth planet. Inter.*, **13**, 260–267.
- Devyatkin, Y.V. & Smelov, S.B., 1980. Position of basalts in the Cenozoic sedimentary sequence of Mongolia, *Int. Geol. Rev.*, **22**, 307–317.
- Dijkstra, A.H., Brouwer, F.M., Cunningham, W.D., Buchan, C., Badarch, G. & Mason, P.R.D., 2006. Late Neoproterozoic proto-arc ocean crust in the Dariv Range, Western Mongolia: a supra-subduction zone end-member ophiolite, *J. Geol. Soc. Lond.*, **163**, 363–373.
- Dunlop, D.J., 2002. Theory and application of the Day plot (Mrs/Ms versus Hcr/Hc) 1. Theoretical curves and tests using titanomagnetite data, *J. Geophys. Res.*, **107**, EPM 4.
- Enkin, R.J., Yang, Z., Chen, Y. & Courtillot, V., 1992. Paleomagnetic constraints on the geodynamic history of the major blocks of China from the Permian to the Present, *J. Geophys. Res.*, **97**, 13,953–13,989.
- Fisher, R.A., 1953. Dispersion on a sphere, *Proc. Roy. Soc. Lond.*, **A217**, 295–305.
- Fleck, R.J., Sutter, J.F. & Elliot, D.H., 1977. Interpretation of discordant $^{40}\text{Ar}/^{39}\text{Ar}$ age-spectra of Mesozoic tholeiotes from Antarctica, *Geochim. Cosmochim. Acta*, **41**, 15–32.
- Garfunkel, Z., 1988. Regional deformation by block translation and rotation, in *Paleomagnetic Rotations and Continental Deformation*, Vol. 254, pp. 181–208, eds Kissel, C. & Laj, C., Nato ASO Series, Kluwer Academic Publishers, Dordrecht, The Netherlands.
- Graham, S.A., Hendrix, M.S., Wang, L.B. & Carroll, A.R., 1993. Collisional successor basins of western China: impact of tectonic inheritance on sand composition, *Geol. Soc. Am. Bull.*, **105**, 323–344.
- Hafkenscheid, E., Wortel, M.J.R. & Spakman, W., 2006. Subduction history of the Tethyan region derived from seismic tomography and tectonic reconstructions, *J. Geophys. Res.*, **111**, B08401, doi: 10.1029/2005JB003791.
- Hallimond, A.F. & Herroun, E.F., 1933. Laboratory determinations of the magnetic properties of certain igneous rocks, *Proc. Roy. Soc.*, **141**, 302–314.
- Hankard, F., Cogné, J.-P. & Kravchinsky, V., 2005. A new Late Cretaceous paleomagnetic pole for the west of Amuria block (Khurmen Uul, Mongolia), *Earth planet. Sci. Lett.*, **236**, 359–373.
- Hankard, F., Cogné, J.-P., Kravchinsky, V., Carporzen, L., Bayasgalan, A. & Lkhagvadorj, P., 2007a. New Tertiary paleomagnetic poles from Mongolia and Siberia at 40, 30, 20, and 13 Ma: clues on the inclination shallowing problem in central Asia, *J. Geophys. Res.*, **112**, B02101, doi:10.1029/2006JB004488.
- Hankard, F., Cogné, J.P., Quidelleur, X., Bayasgalan, A. & Lkhagvadorj, P., 2007b. Paleomagnetism and K–Ar dating of Cretaceous basalts from Mongolia, *Geophys. J. Int.*, doi:10.1111/j.1365-246X.2007.03292.x.
- Helo, C., Hegner, E., Kröner, A., Badarch, G., Tomurtogoo, O., Windley, B.F. & Dulski, P., 2006. Geochemical signature of Paleozoic accretionary complexes of the Central Asian Orogenic Belt in South Mongolia: constraints on arc environments and crustal growth, *Chem. Geol.*, **227**, 236–257.
- Hendrix, M.S., Graham, S.A., Amory, J. & Badarch, G., 1996. Noyon Uul syncline, southern Mongolia: lower Mesozoic sedimentary record of the tectonic amalgamation of central Asia, *Geol. Soc. Am. Bull.*, **108**, 1256–1274.
- Höck, V. et al., 1997. Oligocene–Miocene sediments, fossils and basalts from the Valley of Lakes (Central Mongolia)—an integrated study, *Mitteilungen der Österreichischer Geolischer Gesellschaft*, **90**, 83–125.
- Howard, J.P., Cunningham, W.D., Davies, S.J., Dijkstra, A.H. & Badarch, G., 2003. The stratigraphic and structural evolution of the Dzereg Basin, western Mongolia: clastic sedimentation, transpressional faulting and basin destruction in an intraplate, intracontinental setting, *Basin Res.*, **15**, 45–72.
- Howard, J.P., Cunningham, W.D. & Davies, S.J., 2006. Competing processes of clastic deposition and compartmentalized inversion in an actively evolving transpressional basin, western Mongolia, *J. Geol. Soc. Lond.*, **163**, 657–670.
- Johnson, C.L., 2004. Polyphase evolution of the East Gobi basin: sedimentary and structural records of Mesozoic–Cenozoic intraplate deformation in Mongolia, *Basin Res.*, **16**, 79–99.
- Kim, Y.-S. & Sanderson, D.J., 2006. Structural similarity and variety at the tips in a wide range of strike-slip faults: a review, *Terra Nova*, **18**, 330–344.
- Kirschvink, J.L., 1980. The least-squares line and plane and the analysis of palaeomagnetic data, *Geophys. J. Roy. Astron. Soc.*, **62**, 699–718.
- Koppers, A.A.P., 2002. ArArCALC-software for $^{40}\text{Ar}/^{39}\text{Ar}$ age calculations, *Comput. Geosci.*, **28**, 605–619.
- Mann, P., 2007. Global catalogue, classification, and tectonic origins of restraining and releasing bends on active and ancient strike-slip fault systems, in *Tectonics of Strike-Slip Restraining and Releasing Bends*, eds Cunningham, W.D. & Mann, P., Special Publication of the Geological Society of London, in press.
- McFadden, P.L. & Lowes, F.J., 1981. The discrimination of mean directions drawn from Fisher distributions, *Geophys. J. Roy. Astron. Soc.*, **67**, 19–33.
- McFadden, P.L. & McElhinny, M.W., 1988. The combined analysis of remagnetisation circles and direct observations in paleomagnetism, *Earth planet. Sci. Lett.*, **87**, 161–172.
- McFadden, P.C. & McElhinny, M.W., 1990. Classification of the reversal test in palaeomagnetism, *Geophys. J. Int.*, **103**, 725–729.
- McFadden, P.L., Merrill, R.T., McElhinny, M.W. & Lee, S., 1991. Reversals of the Earth's magnetic field and temporal variations of the dynamo families, *J. Geophys. Res.*, **96**, 3923–3933.
- Meng, Q.-R., Hu, J.-M., Jin, J.-Q. & Xu, D.-F., 2003. Tectonics of the late Mesozoic wide extensional basin system in the China–Mongolia border region, *Basin Res.*, **15**, 397–415.

- Mullender, T.A.T., Van Velzen, A.J. & Dekkers, M.J., 1993. Continuous drift correction and separate identification of ferrimagnetic and paramagnetic contribution in thermomagnetic runs, *Geophys. J. Int.*, **114**, 663–672.
- Nur, A., Ron, H. & Scotti, O., 1988. Mechanics of distributed fault and block rotation, in *Paleomagnetic Rotations and Continental Deformation*, Vol. 254, pp. 209–228, eds Kissel, C. & Laj, C., Nato ASO series, Kluwer Academic Publishers, Dordrecht, The Netherlands.
- Philip, H. & Ritz, J.-F., 1999. Gigantic paleo-landslide associated with active faulting along the Bogd fault (Gobi-Altay, Mongolia), *Geology*, **27**, 211–214.
- Renne, P.R., Swisher, C.C., Deino, A.L., Karner, D.B., Owens, T.L. & DePaolo, D.J., 1998. Intercalibration of standards, absolute ages and uncertainties in $^{40}\text{Ar}/^{39}\text{Ar}$ dating, *Chem. Geol.*, **145**, 117–152.
- Ritz, J.F., Brown, E.T., Bourles, D.L., Philip, H., Schlupp, A., Raisbeck, G.M., Yiou, F. & Enkhtuvshin, B., 1995. Slip rates along active faults estimated with cosmic-ray-exposure dates: application to the Bogd fault, Gobi-Altai, Mongolia, *Geology*, **23**, 1019–1022.
- Ritz, J.-F. et al., 2003. Late Pleistocene to Holocene slip rates for the Gurvan Bulag thrust fault (Gobi-Altay, Mongolia) estimated with ^{10}Be dates, *J. Geophys. Res.*, **108**, 2162, doi:10.1029/2001JB000553.
- Roberts, A.P., Pike, C.R. & Verosub, K.L., 2000. First-order reversal curve diagrams: a new tool for characterizing the magnetic properties of natural samples, *J. Geophys. Res.*, **105**, 28,461–28,475.
- Schettino, A. & Scotese, C.R., 2005. Apparent polar wander paths for the major continents (200 Ma to the present day): a palaeomagnetic reference frame for global tectonic reconstructions, *Geophys. J. Int.*, **163**, 727–759.
- Schlupp, A., 1996. *Néotectonique de la Mongolie occidentale analysée à partir de données de terrain, sismologiques et satellitaires*, Université Louis Pasteur, Strasbourg.
- Scotese, C., 2001. Atlas of Earth history, *PALEOMAP Project*, pp. 52, Arlington, TX.
- Sengör, A.M.C., Natal'in, B.A. & Burtman, V.S., 1993. Evolution of the Altaid tectonic collage and Palaeozoic crustal growth in Eurasia, *Nature*, **364**, 299–306.
- Steiger, R.H. & Jäger, E., 1977. Subcommittee on geochemistry: convention on the use of decay constants in geo- and cosmochronology, *Earth planet. Sci. Lett.*, **36**, 359–362.
- Tapponnier, P. & Molnar, P., 1979. Active faulting and Cenozoic tectonics of the Tien Shan, Mongolia, and Baykal regions, *J. geophys. Res.*, **84**, 3425–3459.
- Tauxe, L. & Kent, D.V., 2004. A simplified statistical model for the geomagnetic field and the detection of shallow bias in paleomagnetic inclinations: was the ancient magnetic field dipolar?, in *Timescales of the Paleomagnetic Field*, *Geophysical Monograph*, Vol. 145, pp. 101–116, eds Channell, J.E.T., Kent, D.V., Lowrie, W., Meert, J.G., American Geophys. Union, Washington, DC.
- Tauxe, L. & Watson, G.S., 1994. The fold test: an eigen analysis approach, *Earth planet. Sci. Lett.*, **122**, 331–341.
- Taylor, G.K., Grocott, J., Pope, A. & Randall, D.E., 1998. Mesozoic fault systems, deformation and fault block rotation in the Andean forearc: a crustal scale strike-slip duplex in the Coastal Cordillera of northern Chile, *Tectonophysics*, **299**, 93–109.
- Taymaz, T., Jackson, J. & McKenzie, D., 1991. Active tectonics of the north and central Aegean Sea, *Geophys. J. Int.*, **106**, 433–490.
- Thomas, J.C., Lanza, R., Kazansky, A., Zykin, V., Semakov, N., Mitrokhin, D. & Delvaux, D., 2002. Paleomagnetic study of Cenozoic sediments from the Zaisan basin (SE Kazakhstan and the Chuya depression (Siberian Altai): tectonic implications for central Asia, *Tectonophysics*, **351**, 119–137.
- Torsvik, T.H., Dietmar Müller, R., Van der Voo, R., Steinberger, B. & Gaina, C., in press. Global plate motion frames: toward a unified model, *Rev. Geophys.*
- Traynor, J.J. & Sladen, C., 1995. Tectonic and stratigraphic evolution of the Mongolian People's Republic and its influence on hydrocarbon geology and potential, *Mar. Petrol. Geol.*, **12**, 35–52.
- van der Voo, R., Spakman, W. & Bijwaard, H., 1999. Mesozoic subducted slabs under Siberia, *Nature*, **397**, 246–249.
- van Hinsbergen, D.J.J., Hafkenscheid, E., Spakman, W., Meulenkamp, J.E. & Wortel, M.J.R., 2005. Nappe stacking resulting from subduction of oceanic and continental lithosphere below Greece, *Geology*, **33**, 325–328.
- Vandamme, D., 1994. A new method to determine paleosecular variation, *Phys. Earth planet. Inter.*, **85**, 131–142.
- Vassallo, R., Ritz, J.-F., Braucher, R. & Carretier, S., 2005. Dating faulted alluvial fans with cosmogenic ^{10}Be in the Gurvan Bogd mountain range (Gobi-Altay, Mongolia): climatic and tectonic implications, *Terra Nova*, **17**, 278–285.
- Vassallo, R., Jolivet, M., Ritz, J.-F., Braucher, R., Larroque, C., Sue, M., Todbileg, M. & Javkhlanbold, D., 2007. Uplift age and rates of the Gurvan Bogd system (Gobi-Altay) by apatite fission track analysis, *Earth planet. Sci. Lett.*, **259**, 333–346.
- Wang, F., Zhou, X.-H., Zhang, L.-C., Ying, J.-F., Zhang, Y.-T., Fu-Yuan, W. & Zhu, R.-X., 2006. Late Mesozoic volcanism in the Great Xing'an Range (NE China): timing and implications for the dynamic setting of NE Asia, *Earth planet. Sci. Lett.*, **251**, 179–198.
- Whitford-Stark, J.L., 1987. *A Survey of Cenozoic Volcanism on Mainland Asia*, pp. 74, Geol. Soc. Am., Boulder
- Wijbrans, J.R., Pringle, M.S., Koppers, A.A.P. & Scheveers, R., 1995. Argon geochronology of small samples using the Vulkana argon laserprobe, *Proc. van de Koninklijke Nederlandse Academie van Wetenschappen, Ser. B*, **98**, 185–218.
- Windley, B.F., Alexeev, D., Xiao, W., Kröner, A. & Badarch, G., 2007. Tectonic models for accretion of the Central Asian Orogenic Belt, *J. Geol. Soc. Lond.*, **164**, 31–47.
- Zhao, X., Coe, R.S., Zhou, Y., Wu, H. & Wang, J., 1990. New paleomagnetic results from northern China: collision and suturing with Siberia and Kazakhstan, *Tectonophysics*, **181**, 43–81.
- Zijderveld, J.D.A., 1967. A.c. demagnetisation of rocks: analysis of results, in *Methods in Palaeomagnetism*, pp. 254–286, eds Collinson, D.W. Creer, K.M. & Runcorn, S.K., Elsevier, Amsterdam.
- Zorin, Y.A., 1999. Geodynamics of the western part of the Mongolia-Okhotsk collisional belt, Trans-Baikal region (Russia) and Mongolia, *Tectonophysics*, **306**, 33–56.

SUPPLEMENTARY MATERIAL

The following supplementary material is available for this article:

Table S1. Full analytical data are given. The isotope ratios are corrected for blanks, mass discrimination, ^{37}Ar and ^{39}Ar decay and nuclear interference reactions. Ages are calculated relative to Drachenfels sanidine of 25.26 Ma (and recalculated from there relative to 28.34 Ma for TCR of Renne et al. (1998)). $^{40}\text{Ar}^*$ (per cent) is the percentage radiogenic ^{40}Ar in each step. $^{39}\text{Ar}_K$ is the percentage of $^{39}\text{Ar}_K$ released in each step with a total of 100 per cent over the full experiment (Excel format).

This material is available as part of the online article from: <http://www.blackwell-synergy.com/doi/abs/10.1111/j.1365-246X.2006.03712.x>

(this link will take you to the article abstract).

Please note: Blackwell Publishing are not responsible for the content or functionality of any supplementary materials supplied by the authors. Any queries (other than missing material) should be directed to the corresponding author for the article.